

Invariant-Feature Subspace Recovery: A New Class of Provable Domain Generalization Algorithms

Haoxiang Wang*

University of Illinois Urbana-Champaign

HWANG264@ILLINOIS.EDU

Gargi Balasubramaniam*

University of Illinois Urbana-Champaign

GARGIB2@ILLINOIS.EDU

Haozhe Si

University of Illinois Urbana-Champaign

HAOZHES3@ILLINOIS.EDU

Bo Li

University of Chicago

BOL@UCHICAGO.EDU

Han Zhao

University of Illinois Urbana-Champaign

HANZHAO@ILLINOIS.EDU

Abstract

Domain generalization asks for models trained over a set of training environments to generalize well in unseen test environments. Recently, a series of algorithms such as Invariant Risk Minimization (IRM) have been proposed for domain generalization. However, [Rosenfeld et al. \(2021\)](#) shows that in a simple linear data model, even if non-convexity issues are ignored, IRM and its extensions cannot generalize to unseen environments with less than d_s+1 training environments, where d_s is the dimension of the spurious-feature subspace. In this work, we propose **Invariant-feature Subspace Recovery (ISR)**: a new class of algorithms to achieve provable domain generalization across the settings of classification and regression problems. First, in the binary classification setup of [Rosenfeld et al. \(2021\)](#), we show that our first algorithm, **ISR-Mean**, can identify the subspace spanned by invariant features from the first-order moments of the class-conditional distributions, and achieve provable domain generalization with d_s+1 training environments. Our second algorithm, **ISR-Cov**, further reduces the required number of training environments to $\mathcal{O}(1)$ using the information of second-order moments. Notably, unlike IRM, our algorithms bypass non-convexity issues and enjoy global convergence guarantees. Next, we extend ISR-Mean to the more general setting of multi-class classification and propose **ISR-Multiclass**, which leverages class information and provably recovers the invariant-feature subspace with $\lceil d_s/k \rceil + 1$ training environments for k -class classification. Finally, for regression problems, we propose **ISR-Regression** that can identify the invariant-feature subspace with $d_s + 1$ training environments. Empirically, we demonstrate the superior performance of our ISRs compared with IRM on synthetic benchmarks. Furthermore, ISRs can be used as simple yet effective post-processing methods for any given black-box feature extractors such as neural nets, and we show they can improve the worst-case accuracy of (pre-)trained models against spurious correlations and group shifts over multiple real-world datasets.

Keywords: Domain Generalization, Out-of-Distribution (OOD) Generalization, Invariant Feature Learning, Spurious Correlations

*. Equal contribution.

1. Introduction

Domain generalization, i.e., out-of-distribution (OOD) generalization, aims to obtain models that can generalize to unseen (OOD) test domains after being trained on a limited number of training domains (Blanchard et al., 2011; Wang et al., 2021b; Zhou et al., 2021; Shen et al., 2021). A series of works try to tackle this challenge by learning the so-called domain-invariant features (i.e., features whose distributions do not change across domains) (Long et al., 2015; Ganin et al., 2016; Hoffman et al., 2018; Zhao et al., 2018, 2019; Tachet des Combes et al., 2020). On the other hand, Invariant Risk Minimization (IRM) (Arjovsky et al., 2019), represents another approach that aims to learn features that induce invariant optimal predictors over training environments. Throughout this work, we shall use the term *invariant features* to denote such features. There is a stream of follow-up works of IRM (Javed et al., 2020; Krueger et al., 2021; Shi et al., 2020; Ahuja et al., 2020; Khezeli et al., 2021; Li et al., 2021, 2022), which propose alternative objectives or extends IRM to different settings as well.

Recently, some theoretical works demonstrate that IRM and its variants fail to generalize to unseen environments, or cannot outperform empirical risk minimization (ERM), in various simple data models (Rosenfeld et al., 2021; Kamath et al., 2021; Ahuja et al., 2021b). For instance, Rosenfeld et al. (2021) considers a simple Gaussian linear data model such that the class-conditional distribution of *invariant features* remains the same across domains, while that of *spurious features* changes across domains. Intuitively, a successful domain generalization algorithm is expected to learn an *optimal invariant predictor*, which relies on only the invariant features and is optimal over the invariant features. To remove the noise introduced by finite samples, these theoretical works generally assume that infinite samples are available per training environment to disregard finite-sample effects, and the main evaluation metric for domain generalization algorithms is the *number of training environments* needed to learn an optimal invariant predictor – this metric is also referred to as *environment complexity* in the literature (Chen et al., 2021). In the case of linear predictors, Rosenfeld et al. (2021) shows that IRM and REx (an alternative objective of IRM proposed in Krueger et al. (2021)) need $E > d_s$ to learn optimal invariant predictors, where E is the number of training environments, and d_s is the dimension of spurious features. In the case of non-linear predictors, they both fail to learn invariant predictors. Notice that the $E > d_s$ condition of IRM can be interpreted as a *linear environment complexity* (i.e., $O(d_s)$ complexity), which is also observed in other recent works (Kamath et al., 2021; Ahuja et al., 2021b; Chen et al., 2021). In this work, we propose a novel approach for domain

Learning Paradigm	Graphical Model	Algorithm	Provable Guarantee (# Environments)	Theorem
Binary Classification	Anti-Causal ($y \rightarrow z_c$)	ISR-MEAN	$\mathcal{O}(d_s)$	Thm. 1
		ISR-COV	$\mathcal{O}(1)$	Thm. 2
k -class Classification		ISR-MULTICLASS	$\mathcal{O}(d_s/k)$	Thm. 3
Regression	Causal ($z_c \rightarrow y$)	ISR-REGRESSION	$\mathcal{O}(d_s)$	Thm. 4

Table 1: Summary of our contributions.

generalization, Invariant-feature Subspace Recovery (ISR): which recovers the subspace

spanned by invariant features, and then fits predictors in this subspace. More concretely, we present algorithms for provable recovery in the settings of both classification and regression problems with their corresponding environment complexities, as summarized in Table 1. We start with the simplest case of binary classification and present two algorithms to realize this approach, ISR-Mean and ISR-Cov, which utilize the first-order and second-order moments (i.e., mean and covariance) of class-conditional distributions, respectively. Under the linear data model of Rosenfeld et al. (2021), we prove that a) ISR-Mean is guaranteed to learn the optimal invariant predictor with $E \geq d_s + 1$ environment, matching the environment complexity of IRM that is proved in Rosenfeld et al. (2021), and b) ISR-Cov reduces the requirement to $E \geq 2$, achieving a constant $O(1)$ environment complexity. Notably, both ISR-Mean and ISR-Cov require fewer assumptions on the data model than IRM, and they both enjoy global convergence guarantees, while IRM does not because of the non-convex formulation of its objective. Furthermore, the ISRs are also more computationally efficient than IRM, since the computation of ISRs involves basically only empirical risk minimization (ERM) with one additional call of an eigen-decomposition solver. Next, we extend ISR-Mean to the setting of multi-class classification and propose ISR-Multiclass, which leverages information from multiple classes to provably recover the invariant-feature subspace from $E \geq \lceil d_s/k \rceil + 1$ environments for k -class classification. We then consider the setting of regression and present ISR-Regression, which provably recovers the invariant-feature subspace in $E \geq d_s + 1$ environments.

Empirically, we conduct studies on a set of challenging synthetic linear benchmarks adapted from Aubin et al. (2021), semi-synthetic image benchmarks with strong spurious correlations (variants of Colored MNIST), and a suite of real-world datasets (two image datasets and one text dataset used in Sagawa et al. (2019), with one additional tabular dataset). Our results on the synthetic benchmarks empirically validate our proved environment complexities, and also demonstrate its superior performance when compared with IRM and its variants. Since the real-world data are highly complex and non-linear, over which the ISR approach cannot be directly applied, we apply ISR on top of the features extracted by the hidden layers of trained neural nets as a post-processing procedure. Experiments show that ISR can consistently increase the worst-case accuracy of the trained models against spurious correlations and group shifts, and this includes models trained by ERM, IRM, Information Bottleneck, reweighting, MixUp, and GroupDRO (Sagawa et al., 2019).

2. Related Work

Domain Generalization. Domain generalization (DG), also known as OOD generalization, aims at leveraging the labeled data from a limited number of training environments to improve the performance of learning models in unseen test environments (Blanchard et al., 2011; Muandet et al., 2013). The simplest approach for DG is empirical risk minimization i.e. ERM (Vapnik, 1992), which minimizes the sum of empirical risks over all training environments. Distributionally robust optimization is another approach (Sagawa et al., 2019; Volpi et al., 2018), which optimizes models over a worst-case distribution that is perturbed around the original distribution. Besides, there are two popular approaches, domain-invariant representation learning and invariant risk minimization, which we will discuss in detail below. In addition to algorithms, there are works that propose theoretical frameworks for DG

(Zhang et al., 2021; Ye et al., 2021), or empirically examine DG algorithms over various benchmarks (Gulrajani and Lopez-Paz, 2021; Koh et al., 2021; Wiles et al., 2021). Notably, some recent works consider DG with temporarily shifted environments (Koh et al., 2021; Ye et al., 2022; Wang et al., 2022a), which is a novel and challenging setting. Besides DG, there are other learning paradigms that involve multiple environments, such as multi-task learning (Caruana, 1997; Wang et al., 2021a) and meta-learning (Finn et al., 2017; Wang et al., 2022b), which do not aim at generalization to OOD environments.

Domain-Invariant Representation Learning. Domain-Invariant representation learning is a learning paradigm widely applied in various tasks. In particular, in domain adaptation (DA), many works aim to learn a representation of data that has an invariant distribution over the source and target domains, adopting methods including adversarial training (Ganin et al., 2016; Tzeng et al., 2017; Zhao et al., 2018) and distribution matching (Ben-David et al., 2007; Long et al., 2015; Sun and Saenko, 2016). The domain-invariant representation approach for DA enjoys theoretical guarantees (Ben-David et al., 2010), but it is also pointed out that issues such as conditional shift should be carefully addressed (Zhao et al., 2019). In domain generalization (Blanchard et al., 2011), since there is no test data (even unlabelled ones) available, models are optimized to learn representations invariant over training environments (Albuquerque et al., 2020; Chen et al., 2021). Notice that many domain-invariant representation learning methods for DA can be easily applied to DG as well (Gulrajani and Lopez-Paz, 2021).

Invariant Risk Minimization. Arjovsky et al. (2019) proposes invariant risk minimization (IRM) that aims to learn invariant predictors over training environments by optimizing a highly non-convex bi-level objective. The authors also reduce the optimization difficulty of IRM by proposing a practical version, IRMv1, with a penalty regularized objective instead of a bi-level one. Alternatives of IRM have also been studied (Ahuja et al., 2020; Li et al., 2022). However, Rosenfeld et al. (2021); Kamath et al. (2021); Ahuja et al. (2021b) theoretically show that these algorithms fail even in simple data models.

Spurious Correlation Mitigation In this work, the focus is on a specific kind of distribution shifts involving robustness to *spurious correlations*: a model should not rely on features that might appear to be *spuriously* correlated with the target variable in certain domains. One would like to learn a model which is robust to these spurious correlations and performs well on *all* subpopulations of data during test time (Sagawa et al., 2019), even where the spurious correlations break. Recent work throws light on the finding that ERM is able to learn both “core” and “spurious” features where appropriate linear probing (Kumar et al., 2022a) may be sufficient to find a good predictor. For example, Kirichenko et al. (2022) demonstrate that re-training the last layer with access to a balanced validation dataset or “deep feature weighting” matches or outperforms state-of-the-art methods like GroupDRO (Sagawa et al., 2019), which explicitly minimizes the worst group loss by leveraging domain membership of every sample. Subsequently, Lee et al. (2022) propose “surgical fine-tuning”, claiming that only fine-tuning the last layer for spurious correlation problems performs better than fine-tuning the entire network. This is part of a broader claim that one should fine-tune only those network parameters which are responsible for the observed distribution shift. Another approach involves contrastive representation learning (Zhang et al., 2022) for improved robustness to spurious correlations in the absence of domain-specific labels. In

the setting of regression, [Rosenfeld et al. \(2022\)](#) make similar claims on ERM learning and perform a domain-specific transformation such that different domains share similar optimal predictors. Other perspectives include [Yao et al. \(2022b\)](#) which introduces C-MixUp for regression, a technique that employs sampling of input points to be linearly interpolated as a data augmentation strategy for better in-domain and out-of-domain generalization. In a parallel work, [Ahuja et al. \(2021a\)](#) and [Li et al. \(2022\)](#) propose an information bottleneck regularizer in the form of a variance penalty on the feature representations to the original ERM and IRM objectives in the learning process, demonstrating improved OOD performance. Note that both C-MixUp and information bottleneck require end-to-end training of the model, as opposed to the computationally efficient post-processing approach introduced in this work.

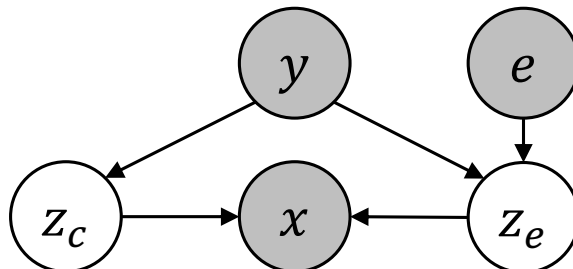


Figure 1: The causal graph of the data model in [Rosenfeld et al. \(2021\)](#). Shading represents that the variable is observed.

3. Problem Setup

Notation Each labeled example can be represented as a (x, y, e) tuple, where $x \in \mathbb{R}^d$ is the input, y is the label which can be discrete or continuous, and $e \in \mathbb{Z}_+$ is the index of the environment that provides (x, y) . In addition, we assume x is generated by a latent feature $z \in \mathbb{R}^d$, which generates x and is correlated with y and e (e.g., see the example in Fig. 1). Besides, we use X, Y, \mathcal{E}, Z to refer to random variables w.r.t. x, y, e, z .

In this paper, we first adopt the linear Gaussian data model of [Rosenfeld et al. \(2021\)](#) for the case of binary classification in Section 4.1.1 and then extend it to the setting of multi-class classification in Section 4.2. We also discuss a new causal model for regression in Section 4.3.

3.1 Binary Classification

As per the linear Gaussian data model of [Rosenfeld et al. \(2021\)](#), it is assumed that the training data are drawn from E training environments, $\mathcal{E} = \{1, \dots, E\}$. For arbitrary training environment $e \in \mathcal{E}$, each sample in this environment is generated by the following mechanism (see Fig. 1 for an illustration): first, a label $y \in \{\pm 1\}$ is sampled,

$$y = \begin{cases} 1, & \text{with probability } \eta \\ -1, & \text{otherwise} \end{cases} \quad (1)$$

Then, both invariant latent features z_c and spurious latent features z_e of this sample are drawn from the following Gaussian distributions:

$$z_c \sim \mathcal{N}(y\mu_c, \sigma_c^2 I) \in \mathbb{R}^{d_c}, z_e \sim \mathcal{N}(y\mu_e, \sigma_e^2 I) \in \mathbb{R}^{d_s} \quad (2)$$

where $\mu_c \in \mathbb{R}^{d_c}, \mu_e \in \mathbb{R}^{d_s}$ and $\sigma_c, \sigma_e \in \mathbb{R}_+$. The constants d_c and d_s refer to the dimension of invariant features and spurious features, respectively. The total number of feature attributes is then $d = d_c + d_s$. Notice that μ_c, σ_c are invariant across environments, while μ_e, σ_e are dependent on the environment index e . Following Rosenfeld et al. (2021), we name $\{\mu_e\}$ and $\{\sigma_e\}$ as *environmental means* and *variances*.

Rosenfeld et al. (2021) adopts a mild non-degeneracy assumption¹ on the environmental mean from the IRM paper (Arjovsky et al., 2019), stated as Assumption 1 below. In addition, the authors also make another non-degeneracy assumption² on the environmental variances, which we relax to the following Assumption 2.

Assumption 1 *The set of environmental means $\{\mu_e\}_{e=1}^E$ is affinely independent.*

Assumption 2 *Assume there exists a pair of distinct training environments $e, e' \in [E]$ such that $\sigma_e \neq \sigma_{e'}$.*

With the latent feature z as a concatenation of z_c and z_e , the observed sample x is generated by a linear transformation on this latent feature. For simplicity, we consider that x has the same dimension as z .

$$z = \begin{bmatrix} z_c \\ z_e \end{bmatrix} \in \mathbb{R}^d, \quad x = Rz = Az_c + Bz_e \in \mathbb{R}^d \quad (3)$$

where $d = d_c + d_s$, and $A = \mathbb{R}^{d \times d_c}, B = \mathbb{R}^{d \times d_s}$ are fixed transformation matrices with concatenation as $R = [A, B] \in \mathbb{R}^{d \times d}$. Then, each observed sample x is effectively a sample drawn from

$$\mathcal{N}(y(A\mu_c + B\mu_e), \sigma_c^2 AA^\top + \sigma_e^2 BB^\top) \quad (4)$$

The following assumption is also imposed on the transformation matrix in Rosenfeld et al. (2021):

Assumption 3 *R is injective.*

Since $R \in \mathbb{R}^{d \times d}$, Assumption 3 leads to the fact $\text{rank}(R) = d$, indicating that R is full-rank.

3.2 Multi-Class Classification

Consider a k class classification problem under the causal graph in Fig. 1. Let y be sampled from a prior distribution of labels $\{y_1, y_2, \dots, y_k\}$. Now, the invariant features $z_c \in \mathbb{R}^{d_c}$ and spurious features $z_e \in \mathbb{R}^{d_s}$ are sampled as follows:

$$z_c \sim \mathcal{N}(\mu_y, \sigma_c^2 I_{d_c}), z_e \sim \mathcal{N}(\mu_{ye}, \sigma_e^2 I_{d_s}) \quad (5)$$

1. It was stated as (9) in Rosenfeld et al. (2021).

2. It is stated as Eq. (10) in Rosenfeld et al. (2021), which is a sufficient (not necessary) condition for our Assumption 2.

where $\mu_y \in \mathbb{R}^{d_c}$, $\mu_{ye} \in \mathbb{R}^{d_s}$ and $\sigma_c, \sigma_e \in \mathbb{R}_+$.

Note that in the binary classification data model discussed in section 3.1, the invariant feature distribution is given by $z_c \sim \mathcal{N}(y\mu_c, \sigma_c^2 I_{d_c})$, where $y \in \{+1, -1\}$. Here, y induces *symmetric means* for the invariant (and similarly spurious features) i.e. $\pm\mu_c$ ($\pm\mu_e$). We will see in section 4.2 that this symmetry assumption is *unnecessary* and artificially increases the environment complexity from $\lfloor d_s/2 \rfloor + 1$ to $d_s + 1$. Thus, we consider a more general and flexible causal model where the means of invariant (and spurious features) depend on the specific value of y .

Finally, the input x is generated from a linear transformation of the concatenated invariant and spurious features as per steps (3) and (4). We also adopt the full-rank assumption on the means of the spurious features from different environments and different classes.

Assumption 4 For the set of environmental means, $\{\mu_{ye}\}_{e=1, y=1}^{E, k}$, we assume that

$$\dim(\text{span}(\{\mu_{ye} : y \in [k], e \in [E]\})) = \min(E \times k, d_s) \quad (6)$$

Intuitively, this assumption ensures that multiple classes / multiple environments do not *trivially replicate* information, and thus the spurious (and thus invariant) subspace can be recovered. When $k = 1$, this assumption is equivalent to Assumption 1.

Finally, we also assume that (3) holds, i.e., R is injective.

3.3 Regression

In the setting of regression, y is a continuous-valued attribute i.e. $y \in \mathbb{R}$. We propose the causal graph³ as shown in Figure 2.

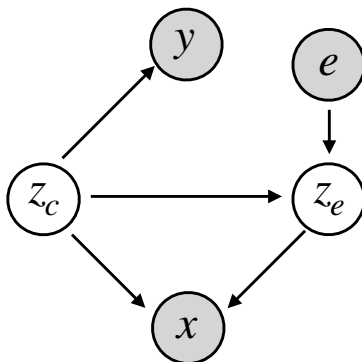


Figure 2: Causal Graph for Regression. Shaded variables are observed.

First, the invariant feature z_c is sampled as follows:

$$z_c \sim \mathcal{N}(\mu_c, \sigma_c^2 I_{d_c}) \quad (7)$$

3. Note that Ahuja et al. (2021a) assume a similar causal model with the difference that all nodes in the graph depend on the environment index e .

where $\mu_c \in \mathbb{R}^{d_c}$, $\sigma_c \in \mathbb{R}_+$. The target y is then determined by a function of z_c :

$$y = f(z_c) = w_c^\top z_c + b_c \in \mathbb{R} \tag{8}$$

Further, the spurious features z_e depend on both the invariant features and the environment index e , which induces a spurious correlation between y and z_c . Specifically,

$$z_e = W_{cs}^e z_c + b_e \in \mathbb{R}^{d_s}, \quad W_{cs}^e \in \mathbb{R}^{d_s \times d_c} \tag{9}$$

Note that W_{cs}^e is an *environment specific* transformation for obtaining the spurious features. Finally, the input x is generated from a linear transformation of the concatenated invariant and spurious features as follows:

$$z = \begin{bmatrix} z_c \\ z_e \end{bmatrix} \in \mathbb{R}^d, \quad x = Rz = Az_c + Bz_e \in \mathbb{R}^d \tag{10}$$

The following assumptions is made in this setting:

Assumption 5 *For every environment, e , W_{cs}^e is full rank, and $d_s \leq d_c$.*

This non-degeneracy assumption ensures that the spurious features z_s have full dimension d_s - since we obtain z_s from z_c via the transformation described in (9), the effective dimension of z_s i.e. d_s cannot be greater than that of the input space i.e., d_c .⁴

Similar to the classification setting, we also make the following assumption on the set of environmental means and the linear map R :

Assumption 6 *The set of environmental means $\{\mu_e\}_{e=1}^E$ is affinely independent and R is injective.*

3.4 Optimal Invariant Predictors and IRM

Denote the data of any training domain e as \mathcal{D}_e . During training, learners have access to the environment index e for each training sample, i.e., learners observe samples in the form of (x, y, e) .

Optimal Invariant Predictors The quest of IRM is to find the optimal invariant predictors, i.e., classifiers/regressors that use only invariant features and are optimal w.r.t. invariant features over the training data. In the data model of Rosenfeld et al. (2021), because of the linear nature of the data generation process, the optimal invariant predictors are contained in the linear function class. If the task of consideration is binary classification, Rosenfeld et al. (2021) chooses the logistic loss as the loss function for optimization⁵, which we also adopt in this work. Then, the goal of domain generalization is to learn a linear

4. Note that our proposed method still holds without the assumption that $d_s \leq d_c$. If W_{cs}^e is not full rank, then the effective dimension of z_s will be smaller than d_s . However, our theorem requires $E > d_s \geq \text{rank}(W_{cs}^e)$, which still holds.

5. Rosenfeld et al. (2021) proves that logistic loss over linear models can attain Bayes optimal classifiers in this data model.

featurizer (feature extractor) Φ and a linear classifier β that minimizes the risk (population loss) on any unseen environment e with data distribution p_e satisfying Assumptions (1)-(3):

$$\mathcal{R}^e(\Phi, \beta) := \mathbb{E}_{(x,y) \sim p^e} \left[\ell \left(w^\top \Phi(x) + b, y \right) \right] \quad (11)$$

where ℓ is logistic loss (for binary classification), cross-entropy loss (for multi-class classification) or squared loss (for regression), and $\beta = (w, b)$ with weight w and bias b .

To be complete, we present the optimal invariant predictor derived by Rosenfeld et al. (2021) in the setting of binary classification as follows:

Proposition 1 (Optimal Invariant Predictor) *Under the data model considered in Eq. (1)-(3), the optimal invariant predictor h^* w.r.t. logistic loss is unique, which can be expressed as a composition of i) a featurizer Φ^* that recovers the invariant features and ii) the classifier $\beta^* = (w^*, b^*)$ that is optimal w.r.t. the extracted features:*

$$h^*(x) = w^{*\top} \Phi^*(x) + b^* \quad (12)$$

$$\Phi^*(x) := \begin{bmatrix} I_{d_c} & 0 \\ 0 & 0 \end{bmatrix} R^{-1}x = \begin{bmatrix} z_c \\ 0 \end{bmatrix} \in \mathbb{R}^{d \times d} \quad (13)$$

$$w^* := \begin{bmatrix} 2\mu_c/\sigma_c^2 \\ 0 \end{bmatrix} \in \mathbb{R}^d, \quad b^* := \log \frac{\eta}{1-\eta} \in \mathbb{R} \quad (14)$$

Notice that even though the optimal invariant predictor h^* is unique, its components (the featurizer and classifier) are only unique up to invertible transformations. For instance, $(w^{*\top} U^{-1})(U\Phi) = w^{*\top} \Phi$ for any invertible $U \in \mathbb{R}^{d \times d}$.

Invariant Risk Minimization IRM optimizes a bi-level objective over a featurizer Φ and a classifier β ,

$$\begin{aligned} \text{IRM} : \quad & \min_{\Phi, \beta} \sum_{e \in [E]} \mathcal{R}^e(\Phi, \beta) \\ & \text{s.t. } \beta \in \arg \min_{\beta} \mathcal{R}^e(\Phi, \beta) \quad \forall e \in [E] \end{aligned} \quad (15)$$

This objective is non-convex and difficult to optimize. Thus, Arjovsky et al. (2019) proposes a Lagrangian form to find an approximate solution,

$$\text{IRMv1} : \min_{\Phi, \hat{\beta}} \sum_{e \in [E]} \mathcal{R}^e(\Phi, \hat{\beta}) + \lambda \left\| \nabla_{\hat{\beta}} \mathcal{R}^e(\Phi, \hat{\beta}) \right\|_2^2 \quad (16)$$

where $\lambda > 0$ controls the regularization strength. Notice that the IRMv1(16) is still non-convex, and it becomes equivalent to the original IRM (15) as $\lambda \rightarrow \infty$.

Environment Complexity To study the dependency of domain generalization algorithms on environments, recent theoretical works (Rosenfeld et al., 2021; Kamath et al., 2021; Ahuja et al., 2021a; Chen et al., 2021) consider the ideal setting of infinite data per training environment to remove the finite-sample effects. In this infinite-sample setting, a core measure of domain generalization algorithms is *environment complexity*: the number of

Algorithm 1 ISR-Mean

Input: Data of all training environments, $\{\mathcal{D}_e\}_{e \in [E]}$.
for $e = 1, 2, \dots, E$ **do**
 Estimate the sample mean of $\{x | (x, y) \in \mathcal{D}_e, y = 1\}$ as $\bar{x}_e \in \mathbb{R}^d$
end for
I. Construct a matrix $\mathcal{M} \in \mathbb{R}^{E \times d}$ with the e -th row as \bar{x}_e^\top for $e \in [E]$
II. Apply PCA to \mathcal{M} to obtain eigenvectors $\{P_1, \dots, P_d\}$ with eigenvalues $\{\lambda_1, \dots, \lambda_d\}$
III. Choose d_s eigenvectors corresponding to the highest eigenvalues and stack them to obtain a transformation matrix $P'' \in \mathbb{R}^{d_s \times d}$. Take the null space of P'' to obtain transformation matrix $P' \in \mathbb{R}^{d_c \times d}$
IV. Fit a linear classifier (with $w \in \mathbb{R}^{d_c}$, $b \in \mathbb{R}$) by ERM over all the training data with transformation $x \mapsto P'x$
Obtain a predictor $f(x) = w^\top P'x + b$

training environments needed to learn an invariant optimal predictor. For this data model, [Rosenfeld et al. \(2021\)](#) proves that with the linear Φ and β , the environment complexity of IRM is $d_s + 1$, assuming the highly non-convex objective (15) is optimized to reach the global optimum. This linear environment complexity (i.e., $\mathcal{O}(d_s)$) of IRM is also proved in ([Kamath et al., 2021](#); [Ahuja et al., 2021a](#)) under different simple data models.

4. Invariant-Feature Subspace Recovery

In this section, we introduce four algorithms for invariant-feature subspace recovery in the setting of binary classification (4.1), multi-class classification (4.2) and regression (4.3). We start with binary classification, where we present ISR-Mean (4.1.1) and ISR-Cov (4.1.2), which recover the invariant-feature subspace with the first-order and second-order moments of class-conditional data distributions, respectively. We then present extensions of ISR-Mean to the setting of multi-class classification (ISR-Multiclass, 4.2) and regression (ISR-Regression, 4.3).

4.1 Binary Classification

4.1.1 ISR-MEAN

Algorithm 1 shows the pseudo-code of ISR-Mean, and we explain its four main steps in detail below. In the setup of Section 3, ISR-Mean enjoys a linear environment complexity that matches that of IRM, while requiring fewer assumptions (no need for Assumption 2).

I. Estimate Sample Means across Environments In any training environment e , each observed sample $x \in \mathbb{R}^d$ is effectively drawn i.i.d. from $\mathcal{N}(y(A\mu_c + B\mu_e), AA^\top\sigma_c^2 + BB^\top\sigma_e^2)$, as stated in (4). In the infinite-sample setting considered in Section 3, the mean of the positive-class data in environment e can be expressed as $\mathbb{E}[X|Y = 1, \mathcal{E} = e]$, which is exactly the value of \bar{x}_e in Algorithm 1. Thus, we know \bar{x}_e satisfies $\bar{x}_e = A\mu_c + B\mu_e$, and the matrix

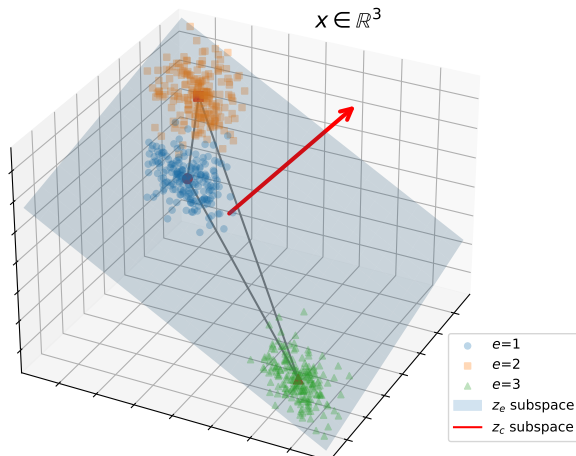


Figure 3: An example for ISR-Mean with $d_c=1$, $d_s=2$, $E=3$. In this \mathbb{R}^3 input space, the blue 2D plane is determined by sample means of positive-class samples of the 3 training environments.

\mathcal{M} can be expressed as

$$\mathcal{M} := \begin{bmatrix} \bar{x}_1^\top \\ \vdots \\ \bar{x}_E^\top \end{bmatrix} = \begin{bmatrix} \mu_c^\top A^\top + \mu_1^\top B^\top \\ \vdots \\ \mu_c^\top A^\top + \mu_E^\top B^\top \end{bmatrix} = \overbrace{\begin{bmatrix} \mu_c^\top & \mu_1^\top \\ \vdots & \vdots \\ \mu_c^\top & \mu_E^\top \end{bmatrix}}^{U^\top :=} R^\top \quad (17)$$

II. PCA on \mathcal{M} . In this step, we apply principal component analysis (PCA) (Pearson, 1901) to the matrix \mathcal{M} . First, PCA performs mean-substraction on \mathcal{M} to shift the sample mean of each column to zero, and we denote the shifted matrix as $\tilde{\mathcal{M}}$. Then, PCA eigen-decompose $\hat{\Sigma}_{\mathcal{M}} := \frac{1}{E} \tilde{\mathcal{M}}^\top \tilde{\mathcal{M}}$, the sample covariance matrix of $\tilde{\mathcal{M}}$, such that $\hat{\Sigma}_{\mathcal{M}} = P^\top S P$, where $P = [P_1, \dots, P_d] \in \mathbb{R}^{d \times d}$ is a stack of eigenvectors $\{P_i\}_{i \in [d]}$, and $S \in \mathbb{R}^{d \times d}$ is a diagonal square matrix with diagonal entries as eigenvalues $\{\lambda_i\}_{i=1}^d$ of $\tilde{\Sigma}_{\mathcal{M}}$. We consider the eigenvalues $\{\lambda_i\}_{i=1}^d$ are sorted in ascending order.

III: Recover the Invariant-Feature Subspace Stack the eigenvectors corresponding to the highest d_s eigenvalues to obtain a transformation matrix $P'' \in \mathbb{R}^{d_s \times d}$. Then, take the null space of this matrix to obtain $P' \in \mathbb{R}^{d_c \times d}$.

Note that when $E \geq d_s + 1$, one can choose the *lowest* d_c eigenvalues and stack the corresponding eigenvectors to obtain a transformation directly into the invariant-feature subspace. However, when $E < d_s + 1$, this will not be equivalent to the presented algorithm, a discussion of which is deferred to section A.1.

IV. Train a Classifier in the Invariant-Feature Subspace In this final step, we just transform all the training data by the transformation $x \mapsto P'x$, and fit a linear classifier with ERM to the transformed data to obtain an predictor,

$$f(x) = w^\top P'x + b \quad (18)$$

which is guaranteed to be the optimal invariant predictor h^* defined in Proposition 1, i.e., $f \equiv h^*$.

Global Convergence Guarantee ISR-Mean is guaranteed to converge to a global optimum since a) the step I and III are optimization-free, b) PCA can be efficiently solved to global the optimum by various methods (Arora et al., 2012; Vu et al., 2013; Hauser et al., 2018; Eftekhari and Hauser, 2020), c) the ERM objective of linear classifiers with logistic loss is convex, enjoying global convergence.

Geometric Interpretation We provide a geometric interpretation of ISR-Mean with a 3D example in Fig. 3, where $d_c=1$, $d_s=2$, $E=3$. For each environment e , the sample mean of its positive-class data, \bar{x}_e , must lie in a d_s -dimensional spurious-feature subspace in the infinite-sample setting, as proved by Theorem 1. ISR-Mean aims to identify this spurious-feature subspace, and take its tangent subspace as the invariant-feature subspace.

Linear Environment Complexity In the infinite-sample setting, we prove below that with more than d_s training environments, ISR-Mean is guaranteed to learn the invariant optimal predictor (Theorem 1). Notice that even though this linear environment complexity is identical to that of IRM (proved in Theorem 5.1 of Rosenfeld et al. (2021)), our ISR-Mean has two additional advantages: (a) Unlike IRM, ISR-Mean does not require any assumption on the covariance⁶ such as Assumption 2; (b) ISR-Mean enjoys the global convergence guarantee, while IRM does not due to its non-convex formulation. The proof is in Appendix A.1.

Theorem 1 (ISR-Mean) *Suppose $E > d_s$ and the data size of each environment is infinite, i.e., $|\mathcal{D}_e| \rightarrow \infty$ for $e=1, \dots, E$. For PCA on the \mathcal{M} defined in (17), the obtained eigenvectors $\{P_1, \dots, P_d\}$ with corresponding ascendingly ordered eigenvalues $\{\lambda_1, \dots, \lambda_d\}$ satisfy*

$$\forall 1 \leq i \leq d_c, \lambda_i = 0 \quad \text{and} \quad \forall d_c < i \leq d, \lambda_i > 0$$

The eigenvectors corresponding to these zero eigenvalues, i.e., $\{P_1, \dots, P_{d_c}\}$, can recover the subspace spanned by the invariant latent feature dimensions, i.e.,

$$\text{Span}(\{P_1^\top R, \dots, P_{d_c}^\top R\}) = \text{Span}(\{\hat{\mathbf{d}}_c^1, \dots, \hat{\mathbf{d}}_c^{d_c}\}) \tag{19}$$

where $\hat{\mathbf{d}}_c^i$ is the unit-vector along the i -th coordinate in the latent feature space for $i = 1, \dots, d_c$. Then, the classifier f fitted with ERM to training data transformed by $x \mapsto [P_1, \dots, P_{d_c}]^\top x$ is guaranteed to be the invariant optimal predictor, i.e., $f = h^$, where h^* is defined in (12).*

4.1.2 ISR-Cov

The pseudo-code of ISR-Cov is presented in Algorithm 2, with a detailed explanation below. In the setup of Section 3, ISR-Cov attains an $\mathcal{O}(1)$ environment complexity, the optimal complexity any algorithm can hope for, while requiring fewer assumptions than IRM (no need for Assumption 1).

6. IRM needs a covariance assumption stronger than our Assumption 2, as pointed out in Sec. 3.

I. Estimate and Select Sample Covariances across Environments As Eq.(4) indicates, in any environment e , each observed sample $x \in \mathbb{R}^d$ with $y = 1$ is effectively drawn i.i.d. from $\mathcal{N}(A\mu_c + B\mu_e, AA^\top\sigma_c^2 + BB^\top\sigma_e^2)$. Thus, the covariance of the positive-class data in environment e can be expressed as $\text{Cov}[X|Y = 1, \mathcal{E} = e] = AA^\top\sigma_c^2 + BB^\top\sigma_e^2$, which is the value that Σ_e in step I of Algorithm 2 estimates. The estimation is exact in the infinite-sample setting of consideration, so we have $\Sigma_e = AA^\top\sigma_c^2 + BB^\top\sigma_e^2$. Assumption 2 guarantees that we can select a pair of environments e_1, e_2 with $\Sigma_1 \neq \Sigma_2$. Then, we have

$$\Delta\Sigma := \Sigma_{e_1} - \Sigma_{e_2} = (\sigma_{e_1}^2 - \sigma_{e_2}^2)BB^\top \in \mathbb{R}^{d \times d} \quad (20)$$

II. Eigen-decompose $\Delta\Sigma$ Similar to the step II of Algorithm 1 explained in Sec. 4.1.1, we eigen-decompose $\Delta\Sigma$ to obtain eigenvectors $\{P_i\}_{i=1}^d$ corresponding to eigenvalues $\{\lambda_i\}_{i=1}^d$. We consider the eigenvalues are sorted in ascending order by their *absolute values*.

III. Recover the Invariant-Feature Subspace As we shall formally prove in Theorem 2, in the infinite-sample setting, a) the eigenvalues $\{\lambda_i\}_{i=1}^d$ should exhibit a ‘‘phase transition’’ phenomenon such that the first d_c eigenvalues all are *zeros* while the rest are all *non-zero*, b) the d_c eigenvectors corresponding to zero eigenvalues, $\{P_1, \dots, P_{d_c}\}$, are guaranteed to recover the d_c -dimensional invariant-feature subspace. We stack these eigenvectors as a matrix P'

$$P' := [P_1, \dots, P_{d_c}]^\top \in \mathbb{R}^{d_c \times d} \quad (21)$$

IV. Train a Classifier in the Invariant-Feature Subspace This final step is the same as the step IV of Algorithm 1 described in Sec. 4.1.1.

Global Convergence Applying the same argument in Sec. 4.1.1, it is clear that ISR-Cov also enjoys the global convergence guarantee: the eigen-decomposition and ERM can both be globally optimized.

Improving the Robustness of ISR-Cov In practice with finite data, Algorithm 2 may be non-robust as σ_e and $\sigma_{e'}$ become close to each other. The noise due to finite samples could obfuscate the non-zero eigenvalues so that they are indistinguishable from the zero eigenvalues. To mitigate such issues, we propose a robust version of ISR-Cov that utilizes more pairs of the given environments. Briefly speaking, the robust version is to **a)** run the step I to III of ISR-Cov over $N \leq \binom{E}{2}$ pairs of environments with distinct sample covariances, leading to N d_c -dimensional subspaces obtained through Algorithm 2, **b)** we find the stable d_c -dimensional subspace, and use it as the invariant-feature subspace that we train the following classifier. Specifically, we achieve b) by computing the flag-mean (Marrinan et al., 2014) over the set of P' (defined in (21)) obtained from the N selected pairs of environments. Compared with the original ISR-Cov, this robust version makes use of training data more efficiently (e.g., it uses more than one pair of training environments) and is more robust in the finite-data case. We implement this robust version of ISR-Cov in our experiments in Sec. 5.

Geometric Interpretation We provide an geometric interpretation of ISR-Cov with a 3D example in Fig. 4, where $d_c=1, d_s=2, E=2$. For either environment $e \in \{1, 2\}$, the covariance of its class-conditional latent-feature distribution, $\begin{bmatrix} \sigma_c^2 I_{d_c} & 0 \\ 0 & \sigma_e^2 I_{d_s} \end{bmatrix}$, is *anisotropic*:

Algorithm 2 ISR-Cov

Input: Data of all training environments, $\{\mathcal{D}_e\}_{e \in [E]}$.
for $e = 1, 2, \dots, E$ **do**
 Estimate the sample covariance of $\{x | (x, y) \in \mathcal{D}_e, y = 1\}$ as $\Sigma_e \in \mathbb{R}^{d \times d}$
end for
I. Select a pair of environments e_1, e_2 such that $\Sigma_1 \neq \Sigma_2$, and compute their difference, $\Delta\Sigma := \Sigma_{e_1} - \Sigma_{e_2}$
II. Eigen-decompose $\Delta\Sigma$ to obtain eigenvectors $\{P_1, \dots, P_d\}$ with eigenvalues $\{\lambda_1, \dots, \lambda_d\}$
III. Stack d_c eigenvectors of eigenvalues with lowest absolute values to obtain a matrix $P' \in \mathbb{R}^{d_c \times d}$
IV. Fit a linear classifier (with $w \in \mathbb{R}^{d_c}$, $b \in \mathbb{R}$) by ERM over all training data with transformation $x \mapsto P'x$
Obtain a predictor $f(x) = w^\top P'x + b$

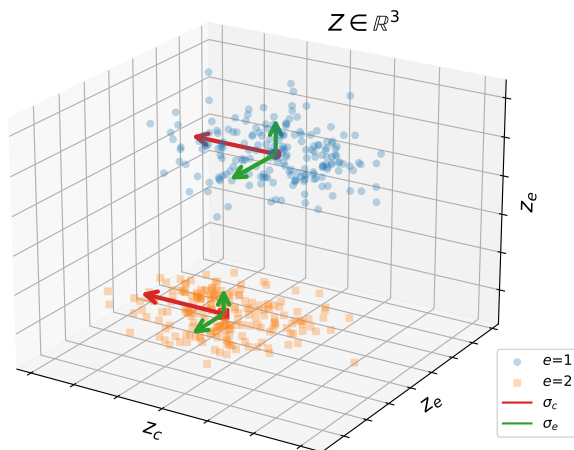


Figure 4: An example for ISR-Cov, where $d_c=1$, $d_s=2$, $E=2$. In this latent feature space of $z \in \mathbb{R}^3$, there is one dimension of z_c and the rest two of z_e .

the variance σ_c along invariant-feature dimensions is constant, while σ_e along the spurious-feature dimensions is various across $e \in \{1, 2\}$ (ensured by Assumption 2). Though the transformation R is applied to latent features, ISR-Cov still can identify the subspace spanned by invariant-feature dimensions in the latent-feature space by utilizing this anisotropy property.

O(1) Environment Complexity In the infinite-sample setting, we prove below that as long as there are at least two training environments that satisfy Assumption 2 and 3, ISR-Cov is guaranteed to learn the invariant optimal predictor. This is the minimal possible environment complexity, since spurious and invariant-features are indistinguishable with only one environment. Notably, unlike IRM, a) ISR-Cov does not require Assumption 1, and b) ISR-Cov has a global convergence guarantee. The proof is in Appendix A.2.

Theorem 2 (ISR-Cov) *Suppose $E \geq 2$ and the data size of each environment is infinite, i.e., $|\mathcal{D}_e| \rightarrow \infty$ for $e=1, \dots, E$. Eigen-decomposing $\Delta\Sigma$ defined in (20), the obtained eigenvectors $\{P_1, \dots, P_d\}$ with corresponding eigenvalues $\{\lambda_1, \dots, \lambda_d\}$ (ascendingly ordered*

by absolute values) satisfy

$$\forall 1 \leq i \leq d_c, \lambda_i = 0 \quad \text{and} \quad \forall d_c < i \leq d, \lambda_i \neq 0$$

The eigenvectors corresponding to these zero eigenvalues, i.e., $\{P_1, \dots, P_{d_c}\}$, can recover the subspace spanned by the invariant latent feature dimensions, i.e.,

$$\text{Span}(\{P_1^\top R, \dots, P_{d_c}^\top R\}) = \text{Span}(\{\hat{\mathbf{d}}_c^1, \dots, \hat{\mathbf{d}}_c^{d_c}\}) \quad (22)$$

where $\hat{\mathbf{d}}_c^i$ is the unit-vector along the i -th coordinate in the latent feature space for $i = 1, \dots, d_c$. Then, the classifier f fitted with ERM to training data transformed by $x \mapsto [P_1, \dots, P_{d_c}]^\top x$ is guaranteed to be the invariant optimal predictor, i.e., $f = h^*$, where h^* is defined in (12).

4.2 ISR-Multiclass

Now, we introduce invariant-feature subspace recovery for multi-class classification. As discussed in section 3.2, the binary *binary* target variable induces *symmetric* means for both the invariant and spurious features. This is not necessary, and we now consider a more general scenario. Moreover, in the more realistic multi-class setting, it is unclear whether there exists any relation between the number of classes and the number of training environments required to recover invariant features. Further, Singla and Feizi (2021) demonstrates that features that are spurious for a given target label may be the core features for another. One could apply class-specific transformations to mitigate this. However, this is infeasible as we do not know the class labels during testing. Thus, we would now like to answer the following question:

In the context of linear causal models, can the number of classes compensate for the number of training environments in recovering the invariant features?

In order to answer the above question, we propose **ISR-Multiclass**, an extension of the ISR-Mean algorithm that provably recovers the invariant subspace in $\lceil d_s/k \rceil + 1$ environments, where d_s is the number of spurious features (i.e., the dimensionality of the spurious-feature subspace) and k is the number of classes. Note that our result improves over the original environmental complexity of $d_s + 1$ for the binary classification problem⁷, hence it provides an affirmative answer to the above problem. Furthermore, our result shows that the benefits of k -class classification problems help to reduce the environmental complexity by an order of k .

The ISR-Multiclass algorithm is outlined in Algorithm 3. First, the detailed steps for the algorithm are presented, followed by a theorem formally stating the improvement in the environment complexity.

I. Estimating Sample Means for Every Environment and Every Class Construct the following matrix \mathcal{M}_k for class k where each row contains the sample mean conditioned on a given environment e , for class k . In other words, each row is $\bar{x}_{ek} = A\mu_k + B\mu_{ke}$. Note

7. When $k = 2$, the environmental complexity in ISR-Mean is $d_s + 1$ instead of $d_s/2 + 1$ because of one specific assumption on the symmetry of the conditional feature distributions, which we also remove in this section.

Algorithm 3 ISR-Multiclass

Input: Data of all training environments, $\{\mathcal{D}_e\}_{e \in [E]}$ across all classes $y \in \{y_1, y_2, \dots, y_k\}$.
for $y = y_1, y_2, \dots, y_k$ **do**
 for $e = 1, 2, \dots, E$ **do**
 Estimate the sample mean of $\{x | (x, y) \in \mathcal{D}_e, y = y_k\}$ as $\bar{x}_{ke} \in \mathbb{R}^d$
 end for
end for
I. Construct k matrices $\mathcal{M}_k \in \mathbb{R}^{E \times d}$ with the e -th row of the k -th matrix as \bar{x}_{ke}^\top for $e \in [E]$
II. Apply PCA to each \mathcal{M}_k to obtain a set of eigenvectors. Choose eigenvectors corresponding to $E - 1$ highest eigenvalues to construct $P_k := [P_{1k} | P_{2k} | \dots | P_{(E-1)k}] \in \mathbb{R}^{d \times (E-1)}$
III. Stack each P_k to obtain $\mathcal{M}_{total} := [P_1 | P_2 | \dots | P_k] \in \mathbb{R}^{d \times (E-1)k}$
IV. Apply SVD of \mathcal{M}_{total} to obtain singular vectors $\{P'_1, \dots, P'_d\}$ with singular values $\{\lambda_1, \dots, \lambda_d\}$
V. Stack d_s singular vectors with the highest singular values to obtain a transformation matrix $P' \in \mathbb{R}^{d_s \times d}$
VI. Apply transformation $x \mapsto P''x$ on the training data and fit a linear classifier (with $w \in \mathbb{R}^{d_c}$, $b \in \mathbb{R}$)
Obtain a predictor $f(x) = w^\top P''x + b$

that in the infinite sample setting considered in this work, this is exactly the mean as per Equation (4).

$$\mathcal{M}_k := \begin{bmatrix} \bar{x}_{1k}^\top \\ \vdots \\ \bar{x}_{Ek}^\top \end{bmatrix} \quad (23)$$

II. Conduct PCA for every \mathcal{M}_k For every class, conduct PCA to obtain eigenvectors $\{P_i\}_{i=1}^d$ corresponding to eigenvalues $\{\lambda_i\}_{i=1}^d$. By assumption 4, this step yields $E - 1$ eigenvectors (-1 from the mean centering in PCA) which correspond to non-zero eigenvalues.

$$P_k := [P_{1k} | P_{2k} | \dots | P_{(E-1)k}] \in \mathbb{R}^{d \times (E-1)} \quad (24)$$

P_{ik} is the i^{th} eigenvector corresponding to a non-zero eigenvalue in the phase transition of \mathcal{M}_k . Thus, P_k recovers spurious dimensions corresponding to class k , as follows from ISR-Mean. Note that unlike ISR-Mean, the condition $E > d_s$ is *not imposed* as information from a single class may not be sufficient to recover all spurious (and thus invariant) features.

III. Stack all P_k and take SVD (Singular Value Decomposition) After obtaining P_k for every class k , stack all P_k to obtain a new matrix \mathcal{M}_{total} as follows:

$$\mathcal{M}_{total} := [P_1 | P_2 | \dots | P_k] \in \mathbb{R}^{d \times (E-1)k} \quad (25)$$

Next, take the SVD of P_k . Note that this step is motivated by the flag-mean (Marrinan et al., 2014) to find the *common spurious subspace* for all class labels.

IV. Extract Spurious Feature Subspace In Theorem 3, we prove that SVD of \mathcal{M}_{total} leads to d_s non zero singular values, where the corresponding vectors $\{P'_1, \dots, P'_{d_s}\}$ recover the underlying spurious subspace. Stack these vectors as a matrix P' :

$$P' := [P'_1, \dots, P'_{d_s}]^\top \in \mathbb{R}^{d_s \times d} \quad (26)$$

V. Train a Classifier in the Null Space of Spurious-Feature Subspace The final step involves training a classifier in the *null space* of the extracted spurious feature subspace, which is the invariant-feature subspace:

$$\text{Col}(P'') = \text{NullSpace}(P') \in \mathbb{R}^{d_c \times d_c} \quad (27)$$

Theorem 3 (ISR-Multiclass) *Suppose $E \geq \lceil d_s/k \rceil + 1$ and the data size of each environment is infinite, i.e., $|\mathcal{D}_e| \rightarrow \infty$ for $e=1, \dots, E$. On performing **SVD** for \mathcal{M}_{total} (defined in (25)), let $\{\lambda_1, \dots, \lambda_d\}$ denote the set of singular values obtained in descending order. Then, the top d_s singular values are strictly positive:*

$$\forall 1 \leq i \leq d_s, \lambda_i > 0$$

The singular vectors corresponding to the top d_s strictly positive singular values $P_{positive} = \{P'_1, \dots, P'_{d_s}\}$ correspond to the d_s spurious dimensions:

$$\text{Span}(\{P_i^\top R : P_i \in P_{positive}\}) = \text{Span}(\{\hat{\mathbf{d}}_s^1, \dots, \hat{\mathbf{d}}_s^{d_s}\}) \quad (28)$$

where the $\hat{\mathbf{d}}_s^i$ denotes the unit vector along the i^{th} dimension of the latent spurious feature space i.e. $i = 1, 2, \dots, d_s$. Consequently, the $\text{NullSpace}([P'_1, \dots, P'_{d_s}]^\top \in \mathbb{R}^{d_s \times d}) = \text{Col}([P''_1, \dots, P''_{d_c}]^\top) \in \mathbb{R}^{d_c \times d}$ corresponds to a transformation matrix which recovers the invariant-feature subspace. Then, the classifier f fitted with ERM to training data transformed by $x \mapsto [P''_1, \dots, P''_{d_c}]^\top x$ is guaranteed to be the invariant optimal predictor, i.e., $f = h^*$, where h^* is defined in (12).

Global Convergence The ISR-Multiclass algorithm involves applying an additional SVD operation over ISR-Mean, which makes the entire process optimization-free: a classifier trained on these features is globally optimal.

Environment Complexity The environment complexity of ISR-Multiclass is $\lceil d_s/k \rceil + 1$ (detailed proof in A.3). The key observation here is that the column space of each P_i matrix for $i \in [k]$ only consists of the span of $\{\mu_{ie}\}_{e=1}^E$. In order to identify the subspace of spurious features, one needs at least d_s linearly independent components. Hence, the only need is to ensure that $(E-1)k \geq d_s$ so that the column space of \mathcal{M}_{total} is full rank. Solving this inequality leads us to the desired bound on the environment complexity. This implies that one can leverage information from *multiple classes* to *reduce* the environment complexity by a factor of $1/k$, as compared to $d_s + 1$ proposed in Section 4.1.1, while only relying on the 1^{st} order moments of the data generating distribution. Intuitively, ISR-Multiclass leverages *additional* information from multiple classes to find the common spurious feature subspace in lesser number of environments.

4.3 Regression

We now study the problem of invariant-feature subspace recovery in the setting of regression. In regression, the target is continuous, which makes it non-trivial to extend the current framework for provable recovery of the invariant-feature subspace in the absence of a discrete class label. Thus, through this section, we answer the following question:

In the context of linear causal models, can we provably recover the invariant-feature subspace when the target is continuous?

To this end, we first identify a *new* causal model which is more natural for studying regression problems and then propose ISR-Regression i.e. **Invariant Feature Subspace Recovery for Regression**. ISR-Regression extends the notion of invariant-feature subspace recovery under the new causal model for regression and requires $d_s + 1$ environments to provably recover the invariant-feature subspace.

Note on causal model for regression Our proposed causal model for studying regression problems is outlined in Figure 2. This causal model specifies that the domain-invariant features z_c causally determine y , which is *natural* for regression problems: one typically observes a dependent variable y corresponding to a set of features x . This is in contrast to previous works modeling regression in the anti-causal setting (Ahuja et al., 2021a) where the causal mechanism between the features and the labels are reversed. Next, there may be spurious (environment-dependent) features z_e which might be correlated with the target y in some environments but are independent of y given z_c , i.e. $y \perp z_e | z_c$. Thus, the aim is to recover the domain invariant feature subspace corresponding to z_c in order to generalize well to new environments during testing, where the correlation with z_e may change or may not even exist.

4.3.1 ISR-REGRESSION

This section introduces the ISR-Regression algorithm, outlined in Algorithm 4. We first discuss the detailed steps for applying ISR-Regression and then present a theorem to provide a formal guarantee on environment complexity.

Intuition for Algorithm 4 Intuitively, Algorithm 4 can be viewed as applying ISR-Mean 1 over the *entire* dataset as opposed to conditioning on a single class. Further, the current data model in 3.3 for regression considers y to be the dependent variable (as is typically assumed in regression). Conducting the PCA on the global input means still helps us in the provable recovery of the spurious and thus invariant-feature subspace. Geometrically, instead of having a particular kind of data distribution *per class* like in ISR-Mean, we now have this structure globally.

Next, let us look at the detailed steps for conducting ISR-Regression:

I. Estimate Sample Means per Environment First, construct the matrix $\mathcal{M} \in \mathbb{R}^{E \times d}$ where every row of the matrix is the mean \bar{x}_e i.e. mean of samples belonging to a specific environment e . Based on the sampling of x as per (10) this row represents an estimate of the distribution mean $A\mu_c + B\mu_e$ where:

$$\mu_e = W_{cs}^e \mu_c + b_e \tag{29}$$

Algorithm 4 ISR-Regression

Input: Data of all training environments, $\{\mathcal{D}_e\}_{e \in [E]}$.

for $e = 1, 2, \dots, E$ **do**

Estimate the sample mean of $\{x | (x, y) \in \mathcal{D}_e\}$ as $\bar{x}_e \in \mathbb{R}^d$

end for

I. Construct matrix $\mathcal{M} \in \mathbb{R}^{E \times d}$ with the e -th row as \bar{x}_e^\top for $e \in [E]$

II. Apply PCA to \mathcal{M} to obtain eigenvectors $\{P_1, \dots, P_d\}$ with eigenvalues $\{\lambda_1, \dots, \lambda_d\}$

III. Choose d_s eigenvectors corresponding to the highest eigenvalues to and stack them to obtain a transformation matrix $P'' \in \mathbb{R}^{d_s \times d}$. Take the null space of P'' to obtain transformation matrix $P' \in \mathbb{R}^{d_c \times d}$

IV. Fit a linear classifier (with $w \in \mathbb{R}^{d_c}$, $b \in \mathbb{R}$) by ERM over all training data with transformation $x \mapsto P'x$

Obtain a predictor $f(x) = w^\top P'x + b$

Now, we know that \bar{x}_e satisfies $\bar{x}_e = A\mu_c + B\mu_e$. Combining this with the fact that $R = [A \ B]$, the matrix \mathcal{M} can be expressed as

$$\mathcal{M} := \begin{bmatrix} \bar{x}_1^\top \\ \vdots \\ \bar{x}_E^\top \end{bmatrix} = \begin{bmatrix} \mu_c^\top A^\top + \mu_1^\top B^\top \\ \vdots \\ \mu_c^\top A^\top + \mu_E^\top B^\top \end{bmatrix} = \overbrace{\begin{bmatrix} \mu_c^\top & \mu_1^\top \\ \vdots & \vdots \\ \mu_c^\top & \mu_E^\top \end{bmatrix}}^{U^\top :=} R^\top \quad (30)$$

II. Apply PCA on \mathcal{M} After computing \mathcal{M} as defined above, apply PCA on \mathcal{M} . This involves mean centering \mathcal{M} to obtain $\tilde{\mathcal{M}}$ where the sample mean is subtracted from every row of \mathcal{M} . This is followed by eigen-decomposition of the sample covariance matrix of $\tilde{\mathcal{M}}$ which is $\hat{\Sigma}_{\mathcal{M}} := \frac{1}{E} \tilde{\mathcal{M}}^\top \tilde{\mathcal{M}}$. This yields a set of d eigenvectors $\{P_1, P_2, \dots, P_d\}$ and corresponding eigenvalues $\{\lambda_1, \lambda_2, \dots, \lambda_d\}$.

III. Obtain Invariant-Feature Subspace from Eigenvectors Stack the eigenvectors corresponding to the highest d_s eigenvalues to obtain a transformation matrix $P'' \in \mathbb{R}^{d_s \times d}$. Then, take the null space of this matrix to obtain $P' \in \mathbb{R}^{d_c \times d}$.

Note that when $E \geq d_s + 1$, one can choose the *lowest* d_c eigenvalues and stack the corresponding eigenvectors to obtain a transformation directly into the invariant-feature subspace. However, when $E < d_s + 1$, this will not be equivalent to the presented algorithm, a discussion of which is discussed in section A.1.

IV. Train a Classifier in the Invariant-Feature Subspace Once the transformation matrix P' has been computed, transform the input training data $x \mapsto P'x$ and fit a linear regressor on top of this transformed data to obtain a predictor $f(x) = w_c^\top x' + b$.

Theorem 4 (ISR-Regression) Suppose $E > d_s$ and the data size of each environment is infinite, i.e., $|\mathcal{D}_e| \rightarrow \infty$ for $e=1, \dots, E$. On performing PCA for \mathcal{M} (defined in (30)), let the $\{\lambda_1, \lambda_2, \dots, \lambda_d\}$ denote eigenvalues sorted in ascending order and $\{P_1, P_2, \dots, P_d\}$ denote

the corresponding eigenvectors. Then, the following property holds:

$$\lambda_i = \begin{cases} 0 & \text{if } 1 \leq i \leq d_c \\ > 0 & \text{if } d_c < i \leq d \end{cases} \quad (31)$$

The eigenvectors P_{zero} corresponding to the d_c zero eigenvalues respectively can recover the invariant-feature subspace:

$$\text{Span}(\{P_i^\top R : P_i \in P_{zero}\}) = \text{Span}(\{\hat{\mathbf{d}}_c^1, \dots, \hat{\mathbf{d}}_c^{d_c}\}) \quad (32)$$

where the $\hat{\mathbf{d}}_c^i$ denotes the unit vector along the i^{th} dimension of the latent invariant feature space i.e. $i = 1, 2, \dots, d_c$. A regressor f fitted with ERM to training data transformed by $x \mapsto [P_1, \dots, P_{d_c}]^\top x$ is guaranteed to be the invariant optimal predictor, i.e., $f = h^*$, where h^* is defined in (12).

The proof can be found in Appendix A.4.

Optimality The ISR-Regression algorithm is globally optimal: applying PCA does not involve local search and other steps in the algorithm are optimization free. Once the invariant-feature subspace is extracted, performing linear regression recovers the globally optimal predictor due to the convex loss function.

Environment Complexity The environment complexity of ISR-Regression is $d_s + 1$, as will be proved in section A.4. This matches that of the original ISR-Mean algorithm in the binary classification setting.

5. Experiments

We conduct experiments on both synthetic and real datasets to examine our proposed algorithms.

5.1 Binary Classification

5.1.1 SYNTHETIC DATASETS: LINEAR UNIT-TESTS

We adopt a set of synthetic domain generalization benchmarks, Linear Unit-Tests (Aubin et al., 2021), which is proposed by authors of IRM and is used in multiple recent works (Koyama and Yamaguchi, 2020; Khezeli et al., 2021; Du et al., 2021). Specifically, we take four classification benchmarks from the Linear Unit-Tests, which are named by Aubin et al. (2021) as Example-2/2s/3/3s. Example-2 and 3 are two binary classification tasks of Gaussian linear data generated in processes similar to the setup of Sec. 3, and they have identity transformation, $R = I$ (see the definition of R in (3)), while Example 2s/3s are their counterparts with R as a random transformation matrix. However, Example-3/3s do not satisfy Assumption 2, thus cannot properly examine our ISR-Cov. Hence, we construct variants of Example-3/3s satisfying Assumption 2, which we name as Example-3'/3s', respectively. We provide specific details of these benchmarks in Appendix B.1.

Example-2: The data generation process for Example-2 follows the Structural Causal Model (Peters et al., 2015), where $P(Y|\mu_c)$ is invariant across environments.

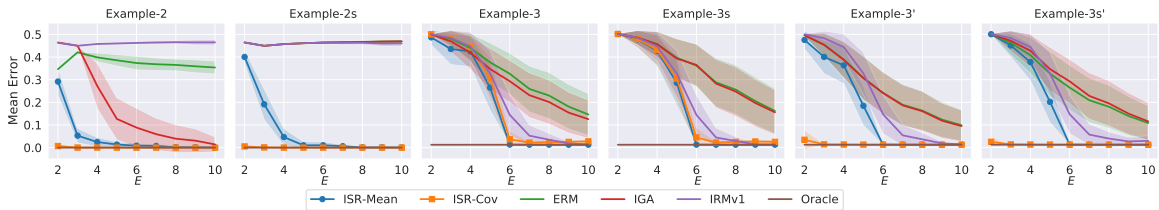


Figure 5: Test results on Linear Unit-Tests (first 4 plots) and its variants (last 2 plots), where $d_c = 5, d_s = 5$, and $E = 2, \dots, 10$.

Example-3: It is similar to our Gaussian setup in 3, except that $\sigma_e \equiv \sigma_c = 0.1$, breaking Assumption 2. In this example, $P(\mu_c|Y)$ is invariant across environments.

Example-3': We modify Example-3 slightly such that $\sigma_c = 0.1$ and $\sigma_e \sim \text{Unif}(0.1, 0.3)$. All the rest settings are identical to Example-3.

Example-2s/3s/3s': A random orthonormal projection matrix $R = [A, B] \in \mathbb{R}^{d \times d}$ (see the definition in (3)) is applied to the original Example-2/3/3' to scramble the invariant and spurious latent feature, leading to Example-2s/3s/3s' with observed data in the form of $x = Az_c + Bz_e$.

Implementation For baseline algorithms, we directly adopt their implementations by Aubin et al. (2021). We implement ISRs following Algorithm 1 and 2, where the last step of fitting predictors is done by the ERM implementation of Aubin et al. (2021), which optimizes the logistic loss with an Adam optimizer (Kingma and Ba, 2015). More details are provided in Appendix B.

Evaluation Procedures Following Aubin et al. (2021), we fix $d=10, d_c=5, d_s=5$, and increase E , the number of training environments, from 2 to 10, with 10K observed samples per environment. Each algorithm trains a linear predictor on these training data, and the predictor is evaluated in E test environments, each with 10K data. The test environments are generated analogously to the training ones, while the spurious features z_e are randomly shuffled across examples within each environment. The mean classification error of the trained predictor over E test environments is evaluated.

Empirical Comparisons We compare our ISRs with several algorithms implemented in Aubin et al. (2021), including IRMv1, IGA (an IRM variant by Koyama and Yamaguchi (2020)), ERM and Oracle (the optimal invariant predictor) on the datasets. We repeat the experiments over 50 random seeds and plot the mean errors of the algorithms. Fig. 5 shows the results of our experiment on these benchmarks: **a)** On Example-2/2s, our ISRs reach the oracle performance with a small E (number of training environments), significantly outperforming other algorithms. **b)** On Example-3/3s, ISRs reach the oracle performance as $E > 5 = d_s$, while IRM or others need more environments to match the oracle. **c)** On Example-3'/3s', ISR-Cov matches the oracle as $E \geq 2$, while the performance of all other algorithms does not differ much from that of Example-3/3s.

Conclusions Observing these results, we can conclude that: **a)** ISR-Mean can stably match the oracle as $E > d_s$, validating the environment complexity proved in Theorem 1.

b) ISR-Cov matches the oracle as $E \geq 2$ in datasets satisfying Assumption 2 (i.e., Example-2/2s/3'/3s'), corroborating its environment complexity proved in Theorem 2.

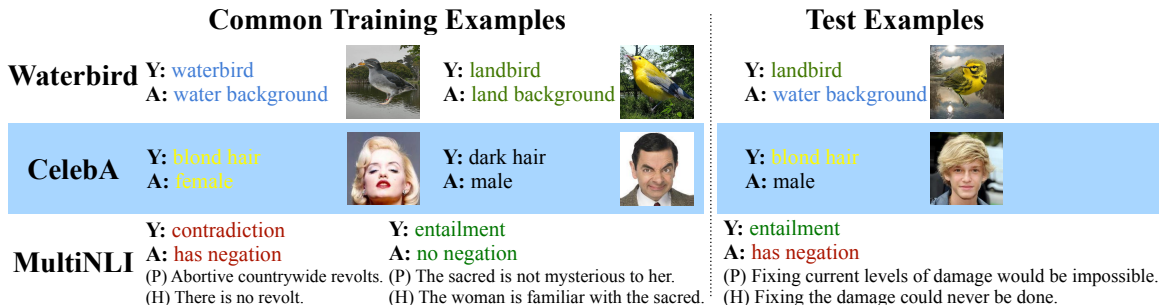


Figure 6: Representative examples of the three real datasets we use. The spurious correlation between the label (**Y**) and the attribute (**A**) in the training data does not hold in the test data.

5.1.2 REAL DATASETS

Dataset	Backbone	Algorithm	Average Accuracy			Worst-Group Accuracy		
			Original	ISR-Mean	ISR-Cov	Original	ISR-Mean	ISR-Cov
Waterbirds	ResNet-50	ERM	86.66±0.67	87.87±0.80	90.47±0.33	62.93±5.37	76.10±1.11	82.46±0.55
		Reweighting	91.49±0.46	91.77±0.52	91.63±0.44	87.69±0.53	88.02±0.42	88.67±0.55
		GroupDRO	92.01±0.33	91.74±0.35	92.25±0.27	90.79±0.47	90.42±0.61	91.00±0.45
CelebA	ResNet-50	ERM	95.12±0.34	94.34±0.12	90.12±2.59	46.39±2.42	55.39±6.13	79.73±5.00
		Reweighting	91.45±0.50	91.38±0.51	91.24±0.35	84.44±1.66	90.08±0.50	88.84±0.57
		GroupDRO	91.82±0.27	91.82±0.27	91.20±0.23	88.22±1.67	90.95±0.32	90.38±0.42
MultiNLI	BERT	ERM	82.48±0.40	82.11±0.18	81.28±0.52	65.95±1.65	72.60±1.09	74.21±2.55
		Reweighting	80.82±0.79	80.53±0.88	80.73±0.90	64.73±0.32	67.87±0.21	66.34±2.46
		GroupDRO	81.30±0.23	81.21±0.24	81.20±0.24	78.43±0.87	78.95±0.95	78.91±0.75

Table 2: Test accuracy(%) with standard deviation of ERM, Re-weighting and GroupDRO over three datasets. We compare the accuracy of original trained classifiers vs. ISR-Mean post-processed classifiers. The average accuracy and the worst-group accuracy are both presented. Bold values mark the higher accuracy over Original vs. ISR-Mean for a given algorithm (e.g., ERM) and a specific metric (e.g., Average Acc.).

We adopt three datasets that Sagawa et al. (2019) proposes to study the robustness of models against spurious correlations and group shifts. See Fig. 6 for a demo of these datasets. Each dataset has multiple spurious attributes, and we treat each spurious attribute as a single environment.

Waterbirds (Sagawa et al., 2019): This is a image dataset built from the CUB (Wah et al., 2011) and Places (Zhou et al., 2017) datasets. The task of this dataset is the classification of waterbirds vs. landbirds. Each image is labelled with class $y \in \mathcal{Y} = \{waterbird, landbird\}$ and environment $e \in \mathcal{E} = \{water\ background, land\ background\}$. Sagawa et al. (2019) defines

Dataset	Backbone	Algorithm	Average Accuracy			Worst-Group Accuracy		
			Linear Probing	ISR-Mean	ISR-Cov	Linear Probing	ISR-Mean	ISR-Cov
Waterbirds	CLIP (ViT-B/32)	ERM	76.42±0.00	90.27±0.09	76.80±0.01	52.96±0.00	71.75±0.39	55.76±0.00
		Reweighting	87.38±0.09	88.23±0.12	88.07±0.05	82.51±0.27	85.13±0.22	83.33±0.00

Table 3: Evaluation with CLIP-pretrained vision transformers. We compare ISR-Mean/ISR-Cov vs. linear probing in the Waterbird dataset, and report the test accuracy (%) with standard deviation.

4 groups⁸ by $\mathcal{G} = \mathcal{Y} \times \mathcal{E}$. There are 4795 training samples, and smallest group (waterbirds on land) only has 56.

CelebA Liu et al. (2015): This is a celebrity face dataset of 162K training samples. Sagawa et al. (2019) considers a hair color classification task ($\mathcal{Y} = \{blond, dark\}$) with binary genders as spurious attributes (i.e., $\mathcal{E} = \{male, female\}$). Four groups are defined by $\mathcal{G} = \mathcal{Y} \times \mathcal{E}$, where the smallest group (blond-haired males) has only 1387 samples.

MultiNLI Williams et al. (2017): This is a text dataset for natural language inference. Each sample includes two sentences, a hypothesis and a premise. The task is to identify if the hypothesis is contradictory to, entailed by, or neutral with the premise ($\mathcal{Y} = \{contradiction, neutral, entailment\}$). Gururangan et al. (2018) observes a spurious correlation between $y=contradiction$ and negation words such as nobody, no, never, and nothing. Thus $\mathcal{E}=\{no\ negation, negation\}$ are spurious attributes (also environments), and 6 groups are defined by $\mathcal{G}=\mathcal{Y} \times \mathcal{E}$. There are 20K training data, while the smallest group (entailment with negations) has only 1521.

Implementation We take three algorithms implemented by Sagawa et al. (2019): ERM, Reweighting, and GroupDRO. First, for each dataset, we train neural nets with these algorithms using the code and optimal hyper-parameters provided by Sagawa et al. (2019) implementation, and early stop models at the epoch with the highest worst-group validation accuracy. Then, we use the hidden-layers of the trained models to extract features of training data, and fit ISR-Mean/Cov to the extracted features. Finally, we replace the original last linear layer with the linear classifier provided by ISR-Mean/Cov, and evaluate it in the test set. More details are provided in Appendix B.

Empirical Comparisons We compare trained models with the original classifier vs. ISR-Mean/Cov post-processed classifiers over three datasets. Each experiment is repeated over 10 random seeds. From the results in Table 2, we can observe that: **a)** ISRs can improve the worst-group accuracy of trained models across all dataset-algorithm choices. **b)** Meanwhile, the average accuracy of ISR-Mean/Cov is maintained around the same level as the original classifier.

5.1.3 REDUCED REQUIREMENT OF ENVIRONMENT LABELS

Algorithms such as GroupDRO are successful, but they require each training sample to be presented in the form (x, y, e) , where the environment label e is usually not available in many

8. Notice that the definition of environment in this paper is different from the definition of group in Sagawa et al. (2019).

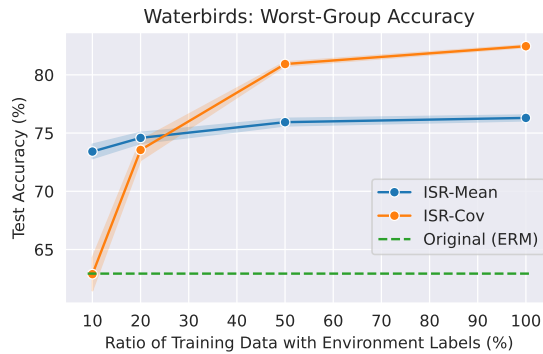


Figure 7: Applying ISR-Mean/ISR-Cov to ERM-trained models with partially available environment labels in the Waterbirds dataset. The shading area indicates the 95% confidence interval for mean accuracy.

real-world datasets. Recent works such as Liu et al. (2021) try to relieve this requirement. To this end, we conduct another experiment on Waterbirds to show that ISRs can be used in cases where only a part of training samples are provided with environment labels. Adopting the same hyperparameter as that of Table 2, we reduce the available environment labels from 100% to 10% (randomly sampled), and apply ISR-Mean/Cov on top of ERM-trained models with the limited environment labels. We repeat the experiment over 10 runs for each of 10 ERM-trained models, and plot the mean accuracy in Fig. 7. We can observe that **a)** even with only 10% environment labels, the worst-group accuracy of ISR-Mean attains 73.4%, outperforming the original ERM-trained classifier by a large margin of 10.5%, and **b)** with 50% environment labels, the worst-group accuracy of ISR-Cov becomes 80.9%, surpassing the original classifier by 18.0%. The compelling results demonstrate another advantage of our ISRs, the *efficient utilization of environment labels*, which indicates that ISRs can be useful to many real-world datasets with only partial environment labels.

5.1.4 APPLYING ISRS TO PRETRAINED FEATURE EXTRACTORS

It is recently observed that CLIP-pretrained models (Radford et al., 2021) have impressive OOD generalization ability across various scenarios (Miller et al., 2021; Wortsman et al., 2022; Kumar et al., 2022b). Also, Kumar et al. (2022b) shows that over a wide range of OOD benchmarks, linear probing (i.e., re-training the last linear layer only) could obtain better OOD generalization performance than finetuning all parameters for CLIP-pretrained models. Notice that ISR-Mean & ISR-Cov also re-train last linear layers on top of provided feature extractors, thus our ISRs can be used as substitutes for linear probing on CLIP-pretrained models. We empirically compare ISR-Mean/Cov vs. linear probing for a CLIP-pretrained vision transformer (ViT-B/32) in the Waterbirds dataset. As Table 3 shows, ISRs outperform linear probing in terms of both average and worst-group accuracy, and the improvement that ISR-Mean obtains is more significant than that of ISR-Cov. This experiment indicates that our ISRs could be useful post-processing tools for deep learning practitioners who frequently use modern pre-trained (foundation) models (Bommasani et al., 2021).

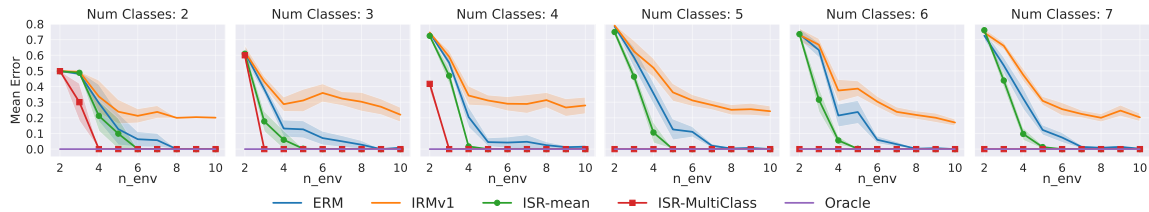


Figure 8: Evaluation on Multiclass Linear Unit Test Example 3s, where the y-axis denotes mean error over the test set. We have fixed $d_s = 5$ and $d_c = 5$, while k varies from 2 to 7. As indicated by our theoretical claim: ISR-Multiclass recovers features roughly in $\lceil d_s/k \rceil + 1$ environments. For example, when $k = 3$, we achieve optimal error in $5/3 + 1 \approx 3$ environments. Similarly, beyond $k = 5$, we achieve optimality in 2 environments itself.

5.2 Multi-Class Classification

We now present the empirical results of ISR-Multiclass for multi-class classification. First, we show improvements on a synthetic multi-class linear unit test followed by the Multi-Class Colored MNIST dataset.

5.2.1 MULTI-CLASS LINEAR UNIT TESTS

We construct a multi-class version of Example 3 (and its scrambled version, Example 3s) as used in [Aubin et al. \(2021\)](#). This is a synthetic dataset based on our causal model in section 3.2. Specific details of our construction can be found in [Appendix B.1](#).

Evaluation Procedures For empirical evaluation, $R \in \mathbb{R}^{d \times d}$ is an orthonormal matrix to consider a harder version of the problem where the inputs are scrambled. The sampling of means μ_k, μ_{ke} is done from a uniform distribution between $[0, 1)$. ν_{inv} and ν_{spu} are the scale of invariant and spurious features. They are set as $\mu_{inv} = 0.1$ and $\mu_{spu} = 1$ as regularization may encourage learning spurious features, making it harder to learn the invariant features. This is similar to Example2 in ([Aubin et al., 2021](#)). Further, $\sigma_c = 0.1, \sigma_e = 0.1, d_s = 5, d_c = 5$. 10,000 are sampled points per environment. k varies from 2 to 7.

Empirical Comparisons Figure 5 depicts the improvement of ISR-Multiclass compared to the original ISR-Mean⁹ and ERM [Vapnik \(1992\)](#). Evaluation is performed on the test split where the spurious dimensions are randomized. The Oracle is trained on this test split. From figure 5, we observe that ISR-Multiclass is indeed able to leverage class information and recover invariant features to achieve optimal error with the number of environments inversely proportional to k , confirmed by our theoretical claim. Especially in the last three plots - with greater classes and lesser environments ($k > 5$ and $n_{env} < 5$), both ISR-Mean and ERM incur *higher* error, but ISR-Multiclass takes advantage of multiple classes to *improve* its performance instead and match the oracle.

9. Note that we condition on a fixed class (0) to enable this comparison.

Algorithm	Average Accuracy		Worst-Group Accuracy		Worst-10 Group Accuracy	
	Original	ISR-Multiclass	Original	ISR-Multiclass	Original	ISR-Multiclass
ERM	58.20 ± 1.03	78.50 ± 0.76	0.00 ± 0.00	21.93 ± 13.40	2.35 ± 0.59	39.60 ± 7.90
IB-ERM	70.58 ± 1.24	81.40 ± 1.15	0.94 ± 1.07	27.36 ± 11.42	10.06 ± 2.66	42.63 ± 6.77
IRM	73.85 ± 0.79	82.01 ± 0.97	8.31 ± 2.55	34.33 ± 9.27	25.66 ± 3.14	45.36 ± 6.46
IB-IRM	77.81 ± 0.84	82.95 ± 2.42	9.73 ± 5.20	32.29 ± 6.66	32.14 ± 2.48	49.17 ± 5.63

Table 4: Evaluation of ISR Multiclass on MC-CMNIST. We report the test accuracy (%) with standard deviation over 5 random trials. A value in bold indicates higher accuracy. ISR-Multiclass outperforms both average and worst group accuracies, especially for ERM. Note that the variance for worst group accuracies is high because of the less number of samples per group (≈ 300).

5.2.2 MULTI-CLASS COLORED MNIST

We consider the 10-class classification task of Colored MNIST as proposed in [Ahuja et al. \(2021a\)](#), which is a semi-synthetic dataset encoding strong spurious correlations between the digit label and color. In the train environments, every digit is highly correlated with a specific color, as depicted in Figure 5.2.2. This correlation breaks down in the test environment, i.e., every digit is randomly colored.

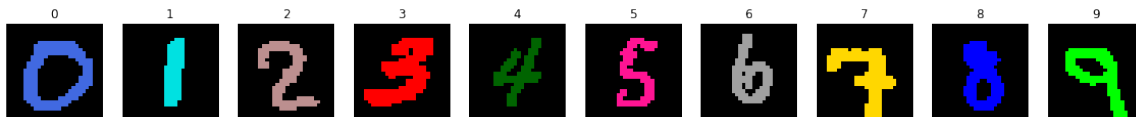


Figure 9: Multiclass Colored MNIST dataset.

Evaluation Procedures Performance is evaluated on every group, which denotes a specific combination of $(y, color) \in \mathcal{G} = \mathcal{Y} \times \mathcal{E}$. Note that there are $10 \times 10 = 100$ groups on this dataset. During training, the samples across input groups are imbalanced owing to the spurious correlation where every digit majorly occurs in its associated color. During test, samples across groups become balanced - thus testing a method’s ability to generalize to minority groups existing in the training set. We report the average accuracy (across all groups), worst group accuracy, and worst-10 group accuracy (average across 10 worst groups). We compare the performance of ISR-Multiclass with ERM, IB-ERM, IRM¹⁰ and IB-IRM which are proposed by [Arjovsky et al. \(2019\)](#) and [Ahuja et al. \(2021a\)](#). The oracle on this dataset achieves 99.03 ± 0.08 average accuracy as per [Ahuja et al. \(2021a\)](#). More details can be found in Appendix B.

Results Table 4 presents the results on MC-CMNIST. It is evident that post-processing with ISR-Multiclass significantly improves both the average and worst-group accuracies, especially prevalent for ERM and IB-ERM. While IRM and IB-IRM perform better than their ERM counterparts, ISR-Multiclass still improves the accuracy by $\approx 5 - 10\%$.

10. To ensure a fair comparison, IRM was re-trained with the groups denoted by digit color.

5.3 Regression

We now study the empirical improvements of ISR-Regression across synthetic and real-life datasets, specifically on a regression Linear Unit Test, Rotated Colored Fashion MNIST, and the Law School dataset.

5.3.1 REGRESSION LINEAR UNIT TEST

We construct a linear unit test based to simulate our data generative model in section 3.3. Specific details of the construction can be found in the appendix B.1.

Implementation Here, $R \in \mathbb{R}^{d \times d}$ is sampled as an orthonormal matrix for transforming x . The invariant mean μ_c is fixed to the vector 1^{d_c} across all environments. The scale of invariant features $\nu_{inv} = 1$ while $\nu_{spu} = 50$ as this makes it harder to learn invariant features under regularization, motivated by a similar argument in Aubin et al. (2021). σ_c is set to 0.1, and 10,000 data points are sampled per environment. The dimensionality d_c is fixed to 5 while d_s is varied from 3 to 6.

Evaluation Procedures For all the methods which will be presented, hyper-parameter search is performed over 20 data seeds and 5 model trials. During training, Adam (Kingma and Ba, 2014) is used as the optimizer and the lowest mean validation error across environments is used for model selection.

Figure 10 presents the empirical evaluation on the linear unit test for regression. Here, the oracle is trained on the test split, where the spurious dimensions are randomized.

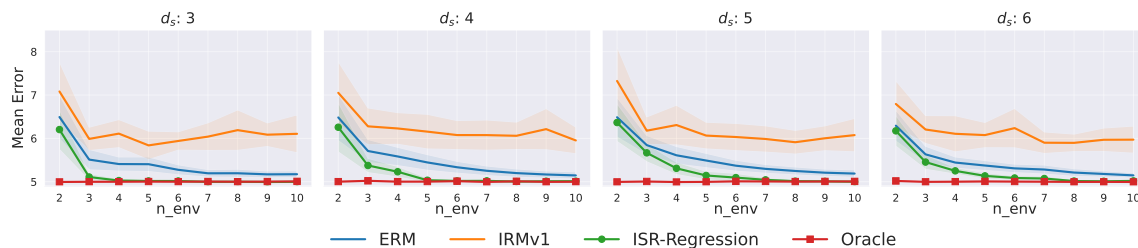


Figure 10: Evaluation on Regression Linear Unit Test, where the y-axis denotes mean error over the test set. The invariant dimension is fixed as $d_c = 5$ and the spurious dimensionality d_s varies from 3 to 6 (top left to bottom right). As indicated by the theoretical claim: ISR-Regression recovers invariant features roughly in $d_s + 1$ environments, matching the performance of the Oracle beyond this number. For example, when $d_s = 3$, optimal performance is achieved in $3 + 1 = 4$ environments.

Results It can be observed that as the dimensionality of the spurious features is increased, the performance of ISR-Regression accordingly matches the environment complexity as proved in Theorem 4. Beyond $E \geq d_s + 1$, ISR-Regression matches the oracle and achieves optimal error implying successful recovery of the invariant-feature subspace. Note that when the spurious features are greater in number i.e. $d_s \geq d_c$, it may be difficult to match the

oracle exactly at this inflection point, possibly due to greater scale and noise in the input corresponding to the spurious dimensions ($\nu_{spu} > \nu_{inv}$). Next, even in the regime of $E < d_s$, ISR-Regression achieves lower error than both ERM and IRMv1. It is interesting to note that IRMv1 performs even worse than ERM, which is possible as invariant penalties based on training error (like in IRMv1) may learn solutions relying on spurious features.

5.3.2 ROTATED COLORED FASHION MNIST

Next, let us consider the Rotated Colored Fashion MNIST dataset, or RCFMNIST in short. This is a semi-synthetic dataset proposed by Yao et al. (2022a) which encodes strong spurious correlations between rotation and color. Formally, the task is to predict the degree of rotation of the object i.e. y represents the angle of rotation between 0 and 360 degrees. The color of the object is spuriously correlated with the degree of rotation: during training, higher the degree, greater is the amount of red in the image. However, during test time, this correlation does not exist - degree is no more correlated with the color. Therefore, any learner relying on the spurious color attribute will perform poorly on the test set, especially on groups which are present in minority during training (where the spurious correlation does not hold). Note that this is a slightly modified version from the setting considered in Yao et al. (2022a) where there exists a *reverse* spurious correlation on test. Figure 11 depicts this concept via a sample of the training set.

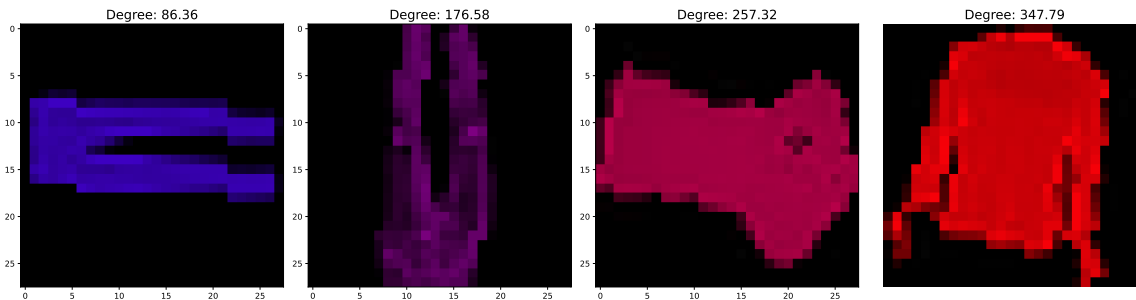


Figure 11: Rotated Colored Fashion MNIST dataset. The rotation of the object increases on moving from left to right. In the training set, a higher degree implies greater amount of red. This trend does not hold during testing. Note that the degree of this spurious correlation is set to 0.8.

Obtaining Discrete Environments It should be noted that the color varies continuously with the target variable (angle of rotation) while ISR-Regression and IRM require a set of discrete environments. To address this, the environments were formed by obtaining the *mean red pixel value* and grouping images based on this value into groups of 10.

Implementation A pretrained ResNet18 (He et al., 2016) is finetuned on this dataset, producing a representation of dimension 512 over which ISR is applied. For training, a batch size of 64 is used for ERM, MixUp and C-MixUp. For IRMv1, the batch size is increased to 128 to ensure all groups are represented in a given batch. The model is trained for 30 epochs using the Adam (Kingma and Ba, 2014) optimizer with a learning rate of

$7e^{-5}$. Hyper-parameters and implementation for ERM, MixUp and C-MixUp are chosen as suggested originally by Yao et al. (2022a)¹¹ and by Aubin et al. (2021) for IRMv1. For tuning the hyper-parameters of ISR (number of spurious dimensions to be scaled down and the degree of scaling), performance on the validation set is used.

Results Table 5.3.2 presents the results from the empirical evaluation of post-processing neural network representations with ISR-Regression. Note that a group here refers to the discrete environment obtained via binning of the red pixel values. The worst group would correspond to those subpopulations of the input data where the spurious correlation breaks (e.g. images with a higher degree in test but with a lower red value). The performance is compared for ERM, IRM, and 2 variants of MixUp as proposed by Yao et al. (2022a). MixUp is a data augmentation strategy that chooses 2 samples and adds their linear interpolation during training. C-MixUp improves on this by smartly sampling pairs that are more similar to each other w.r.t the continuous label. Note that the Oracle on this dataset obtains an average root mean squared error i.e. RMSE 0.112 ± 0.011 and a worst-group RMSE of 0.164 ± 0.048 .

Algorithm	Average RMSE		Worst-Group RMSE	
	Original	ISR-Regression	Original	ISR-Regression
ERM	0.262 ± 0.007	0.247 ± 0.001	0.291 ± 0.012	0.270 ± 0.009
MixUp	0.250 ± 0.004	0.245 ± 0.002	0.268 ± 0.008	0.263 ± 0.005
C-MixUp	0.260 ± 0.014	0.248 ± 0.008	0.293 ± 0.038	0.271 ± 0.019
IRM	0.255 ± 0.006	0.255 ± 0.005	0.277 ± 0.007	0.273 ± 0.009

It can be observed that post-processing with ISR-Regression consistently improves performance on average and for the worst-group root mean squared error i.e. RMSE. Further, it should be noted that this improvement is *greatest* for *weaker* methods such as ERM and C-MixUp, which originally have the lowest performance. For stronger methods like MixUp, the improvement observed is lesser. An interesting point to observe is that C-MixUp performs worse than MixUp on this dataset, possibly because when considering ‘similar’ points to sample by choosing similar label values, a correlation between the color and label can be learnt during this interpolation. Finally, for IRM (which leverages the domain information) the average performance remains similar while the worst-group performance increases, throwing light on the capability of ISR-Regression to improve performance across a spectrum of learners, even when they already leverage domain information.

5.3.3 LAW SCHOOL

Next, evaluation is presented on the LawSchool dataset (Kearns et al., 2018). Law School is a real life tabular dataset consisting of details of people taking the bar exam along with their undergrad GPA, age, race, gender etc. For evaluation, the prediction target is the undergrad GPA or UGPA which is a continuous value between 0 and 4. The protected attribute \mathcal{A} is considered to be the gender. In order to test for robustness to spurious correlations, the

11. <https://github.com/huaxiuyao/C-Mixup>

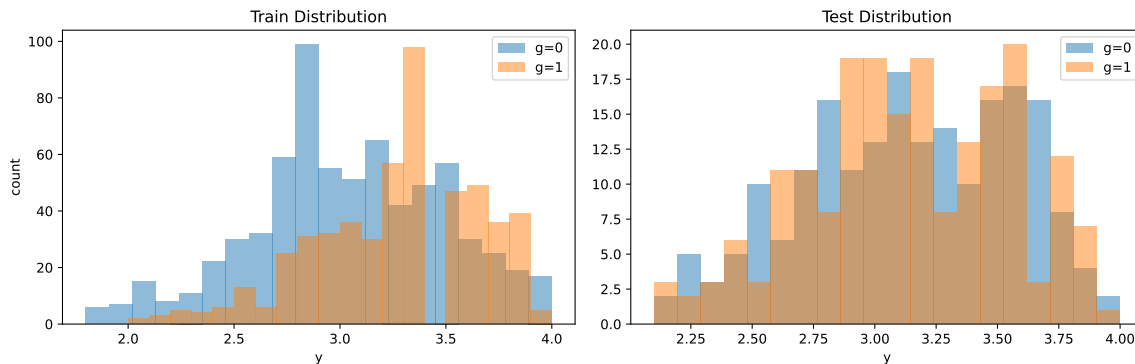


Figure 12: Law School dataset. During training (left), the target y is higher for gender $g = 1$ as compared to $g = 0$. This does not hold during testing (right).

original dataset is modified such that the training set is skewed: the ratio of people with a UGPA > 3 v/s those with UGPA < 3 is higher for people with gender $\mathcal{A} = 1$, as compared to $\mathcal{A} = 0$. This trend does not hold during testing. Figure 12 presents a summary of this shift.

Implementation A publicly available version ¹² of the LawSchool dataset has been used for evaluation, where re-sampling was done for the train, validation and test sets to simulate the spurious correlation as illustrated above. A three layer ReLU neural network was considered for this task trained with the Adam (Kingma and Ba, 2014) optimizer with a learning rate of 0.001. The network was trained for a maximum of 200 epochs for ERM and Reweighting. For GroupDRO, the model was trained for 500 with a weight decay of 0.0001 and $\eta = 0.001$, based on performance on a held-out validation set. For applying ISR-Regression, PCA was first applied to the learnt neural network embeddings of size 30 to down-sample to size 10 and remove noisy features. Similarly, spurious dimensions were first extracted and scaled to 0.

Results Table 5 presents results for evaluation on the LawSchool dataset. For all methods, we report the R-squared metric on the fair test dataset. Note that the Oracle was trained on the test set. A group here denotes membership to a specific gender $g = 0$ or $g = 1$.

The ISR-Regression algorithm is used as a post-processing technique on top of neural network embeddings learnt by ERM, Reweighting and GroupDRO. In Reweighting, the group membership information is used to re-weight each sample with the weight of the corresponding group to which it belongs, thus re-weighting the overall loss to be minimized. Similarly, in GroupDRO, the reweighting happens dynamically by minimizing the worst-group loss at each step.

It can be observed that post-processing with ISR-Regression improves the test R^2 on an average across all groups as well as on the worst-group test set. Note that while Reweighting and GroupDRO outperform ERM on the worst-group (due to balancing out of the sample weights), ISR-Regression still improves the performance and helps close the gap of existing methods with respect to the Oracle, especially for the worst-groups on test.

12. <https://github.com/algowatchpenn/GerryFair/blob/master/dataset/lawschool.csv>

Algorithm	Average Test R^2		Worst-Group Test R^2	
	Original	ISR-Regression	Original	ISR-Regression
ERM	0.224 \pm 0.019	0.239 \pm 0.007	0.163 \pm 0.021	0.193 \pm 0.004
Reweighting	0.231 \pm 0.012	0.249 \pm 0.039	0.173 \pm 0.011	0.212 \pm 0.051
GroupDRO	0.209 \pm 0.014	0.227 \pm 0.005	0.172 \pm 0.014	0.193 \pm 0.001
Oracle	0.321 \pm 0.004		0.299 \pm 0.007	

Table 5: Evaluation of ISR Regression on LawSchool. The test R^2 is reported where a higher value denotes better performance. Note that the Oracle is trained on the test set.

6. Conclusion

In this work, we propose ISR: a new class of algorithms for provable invariant-feature subspace recovery across the settings of classification and regression. Starting with binary classification, under a common data generative model in the literature, we propose two algorithms, ISR-Mean and ISR-Cov, to achieve domain generalization by recovering the invariant-feature subspace. We prove that ISR-Mean admits an $d_s + 1$ environment complexity and ISR-Cov obtains an $\mathcal{O}(1)$ environment complexity, the minimum environment complexity that any algorithm can hope for. Furthermore, both algorithms are computationally efficient, free of local minima, and can be used off-the-shelf as a post-processing method over features learned from existing models. Next, we propose ISR-Multiclass which further improves the environment complexity to $\lceil d_s/k \rceil + 1$ for a k -class classification problem, thus leveraging class information. We then present ISR-Regression for provable recovery in the setting of regression, which enjoys an environment complexity of $d_s + 1$. Empirically, we test our algorithms on synthetic and semi-synthetic benchmarks and demonstrate their superior performance when compared with other domain generalization algorithms. We also show that our proposed algorithms can be used as computationally efficient post-processing methods to increase the worst-case accuracy of (pre-)trained models by testing them on four real-world datasets spanning across image, text and tabular datasets.

References

- Kartik Ahuja, Karthikeyan Shanmugam, Kush Varshney, and Amit Dhurandhar. Invariant risk minimization games. In *International Conference on Machine Learning*, pages 145–155. PMLR, 2020.
- Kartik Ahuja, Ethan Caballero, Dinghuai Zhang, Jean-Christophe Gagnon-Audet, Yoshua Bengio, Ioannis Mitliagkas, and Irina Rish. Invariance principle meets information bottleneck for out-of-distribution generalization. In A. Beygelzimer, Y. Dauphin, P. Liang, and J. Wortman Vaughan, editors, *Advances in Neural Information Processing Systems*, 2021a.
- Kartik Ahuja, Jun Wang, Amit Dhurandhar, Karthikeyan Shanmugam, and Kush R. Varshney. Empirical or invariant risk minimization? a sample complexity perspective. In *International Conference on Learning Representations*, 2021b. URL https://openreview.net/forum?id=jrA5GAccy_.
- Isabela Albuquerque, João Monteiro, Mohammad Darvishi, Tiago H. Falk, and Ioannis Mitliagkas. Generalizing to unseen domains via distribution matching, 2020.
- Martin Arjovsky, Léon Bottou, Ishaan Gulrajani, and David Lopez-Paz. Invariant risk minimization. *arXiv preprint arXiv:1907.02893*, 2019.
- Raman Arora, Andrew Cotter, Karen Livescu, and Nathan Srebro. Stochastic optimization for pca and pls. In *2012 50th Annual Allerton Conference on Communication, Control, and Computing (Allerton)*, pages 861–868. IEEE, 2012.
- Benjamin Aubin, Agnieszka Slowik, Martin Arjovsky, Leon Bottou, and David Lopez-Paz. Linear unit-tests for invariance discovery. *arXiv preprint arXiv:2102.10867*, 2021.
- Sara Beery, Grant Van Horn, and Pietro Perona. Recognition in terra incognita. In *Proceedings of the European conference on computer vision (ECCV)*, pages 456–473, 2018.
- Shai Ben-David, John Blitzer, Koby Crammer, Fernando Pereira, et al. Analysis of representations for domain adaptation. *Advances in neural information processing systems*, 19: 137, 2007.
- Shai Ben-David, John Blitzer, Koby Crammer, Alex Kulesza, Fernando Pereira, and Jennifer Wortman Vaughan. A theory of learning from different domains. *Machine learning*, 79(1):151–175, 2010.
- Gilles Blanchard, Gyemin Lee, and Clayton Scott. Generalizing from several related classification tasks to a new unlabeled sample. *Advances in neural information processing systems*, 24:2178–2186, 2011.
- Rishi Bommasani, Drew A Hudson, Ehsan Adeli, Russ Altman, Simran Arora, Sydney von Arx, Michael S Bernstein, Jeannette Bohg, Antoine Bosselut, Emma Brunskill, et al. On the opportunities and risks of foundation models. *arXiv preprint arXiv:2108.07258*, 2021.
- Rich Caruana. Multitask learning. *Machine learning*, 28(1):41–75, 1997.

- Yining Chen, Elan Rosenfeld, Mark Sellke, Tengyu Ma, and Andrej Risteski. Iterative feature matching: Toward provable domain generalization with logarithmic environments. *arXiv preprint arXiv:2106.09913*, 2021.
- Jacob Devlin, Ming-Wei Chang, Kenton Lee, and Kristina Toutanova. BERT: Pre-training of deep bidirectional transformers for language understanding. In *Proceedings of the 2019 Conference of the North American Chapter of the Association for Computational Linguistics: Human Language Technologies, Volume 1 (Long and Short Papers)*, pages 4171–4186, Minneapolis, Minnesota, June 2019. Association for Computational Linguistics. doi: 10.18653/v1/N19-1423.
- Xin Du, Subramanian Ramamoorthy, Wouter Duivesteijn, Jin Tian, and Mykola Pechenizkiy. Beyond discriminant patterns: On the robustness of decision rule ensembles. *arXiv preprint arXiv:2109.10432*, 2021.
- Armin Eftekhari and Raphael A Hauser. Principal component analysis by optimization of symmetric functions has no spurious local optima. *SIAM Journal on Optimization*, 30(1): 439–463, 2020.
- Chelsea Finn, Pieter Abbeel, and Sergey Levine. Model-agnostic meta-learning for fast adaptation of deep networks. In *ICML*, 2017.
- Yaroslav Ganin, Evgeniya Ustinova, Hana Ajakan, Pascal Germain, Hugo Larochelle, François Laviolette, Mario Marchand, and Victor Lempitsky. Domain-adversarial training of neural networks. *The journal of machine learning research*, 17(1):2096–2030, 2016.
- Ishaan Gulrajani and David Lopez-Paz. In search of lost domain generalization. *arXiv preprint arXiv:2007.01434*, 2020.
- Ishaan Gulrajani and David Lopez-Paz. In search of lost domain generalization. In *International Conference on Learning Representations*, 2021.
- Suchin Gururangan, Swabha Swayamdipta, Omer Levy, Roy Schwartz, Samuel Bowman, and Noah A. Smith. Annotation artifacts in natural language inference data. In *Proceedings of the 2018 Conference of the North American Chapter of the Association for Computational Linguistics: Human Language Technologies, Volume 2 (Short Papers)*, pages 107–112, New Orleans, Louisiana, June 2018. Association for Computational Linguistics. doi: 10.18653/v1/N18-2017.
- Raphael A Hauser, Armin Eftekhari, and Heinrich F Matzinger. Pca by determinant optimisation has no spurious local optima. In *KDD*, pages 1504–1511, 2018.
- Kaiming He, Xiangyu Zhang, Shaoqing Ren, and Jian Sun. Deep residual learning for image recognition. In *Proceedings of the IEEE conference on computer vision and pattern recognition*, pages 770–778, 2016.
- Judy Hoffman, Eric Tzeng, Taesung Park, Jun-Yan Zhu, Phillip Isola, Kate Saenko, Alexei Efros, and Trevor Darrell. Cycada: Cycle-consistent adversarial domain adaptation. In *International conference on machine learning*, pages 1989–1998. PMLR, 2018.

- Khurram Javed, Martha White, and Yoshua Bengio. Learning causal models online. *arXiv preprint arXiv:2006.07461*, 2020.
- Pritish Kamath, Akilesh Tangella, Danica Sutherland, and Nathan Srebro. Does invariant risk minimization capture invariance? In *International Conference on Artificial Intelligence and Statistics*, pages 4069–4077. PMLR, 2021.
- Michael Kearns, Seth Neel, Aaron Roth, and Zhiwei Steven Wu. Preventing fairness gerrymandering: Auditing and learning for subgroup fairness. In *International conference on machine learning*, pages 2564–2572. PMLR, 2018.
- Kia Khezeli, Arno Blaas, Frank Soboczenski, Nicholas Chia, and John Kalantari. On invariance penalties for risk minimization. *arXiv preprint arXiv:2106.09777*, 2021.
- Diederik P Kingma and Jimmy Ba. Adam: A method for stochastic optimization. *arXiv preprint arXiv:1412.6980*, 2014.
- Diederik P. Kingma and Jimmy Ba. Adam: A method for stochastic optimization. In *ICLR*, 2015.
- Polina Kirichenko, Pavel Izmailov, and Andrew Gordon Wilson. Last layer re-training is sufficient for robustness to spurious correlations. *arXiv preprint arXiv:2204.02937*, 2022.
- Pang Wei Koh, Shiori Sagawa, Henrik Marklund, Sang Michael Xie, Marvin Zhang, Akshay Balsubramani, Weihua Hu, Michihiro Yasunaga, Richard Lanus Phillips, Irena Gao, et al. Wilds: A benchmark of in-the-wild distribution shifts. In *International Conference on Machine Learning*, pages 5637–5664. PMLR, 2021.
- Masanori Koyama and Shoichiro Yamaguchi. Out-of-distribution generalization with maximal invariant predictor. *arXiv preprint arXiv:2008.01883*, 2020.
- David Krueger, Ethan Caballero, Joern-Henrik Jacobsen, Amy Zhang, Jonathan Binas, Dinghuai Zhang, Remi Le Priol, and Aaron Courville. Out-of-distribution generalization via risk extrapolation (rex). In *International Conference on Machine Learning*, pages 5815–5826. PMLR, 2021.
- Ananya Kumar, Aditi Raghunathan, Robbie Jones, Tengyu Ma, and Percy Liang. Fine-tuning can distort pretrained features and underperform out-of-distribution. *arXiv preprint arXiv:2202.10054*, 2022a.
- Ananya Kumar, Aditi Raghunathan, Robbie Matthew Jones, Tengyu Ma, and Percy Liang. Fine-tuning can distort pretrained features and underperform out-of-distribution. In *International Conference on Learning Representations*, 2022b. URL <https://openreview.net/forum?id=UYneFzXSJWh>.
- Yoonho Lee, Annie S Chen, Fahim Tajwar, Ananya Kumar, Huaxiu Yao, Percy Liang, and Chelsea Finn. Surgical fine-tuning improves adaptation to distribution shifts. *arXiv preprint arXiv:2210.11466*, 2022.

- Bo Li, Yezhen Wang, Shanghang Zhang, Dongsheng Li, Kurt Keutzer, Trevor Darrell, and Han Zhao. Learning invariant representations and risks for semi-supervised domain adaptation. In *Proceedings of the IEEE/CVF Conference on Computer Vision and Pattern Recognition*, pages 1104–1113, 2021.
- Bo Li, Yifei Shen, Yezhen Wang, Wenzhen Zhu, Dongsheng Li, Kurt Keutzer, and Han Zhao. Invariant information bottleneck for domain generalization. In *Proceedings of the AAAI Conference on Artificial Intelligence*, volume 36, pages 7399–7407, 2022.
- Evan Z Liu, Behzad Haghgoo, Annie S Chen, Aditi Raghunathan, Pang Wei Koh, Shiori Sagawa, Percy Liang, and Chelsea Finn. Just train twice: Improving group robustness without training group information. In *International Conference on Machine Learning*, pages 6781–6792. PMLR, 2021.
- Ziwei Liu, Ping Luo, Xiaogang Wang, and Xiaoou Tang. Deep learning face attributes in the wild. In *Proceedings of International Conference on Computer Vision (ICCV)*, December 2015.
- Mingsheng Long, Yue Cao, Jianmin Wang, and Michael Jordan. Learning transferable features with deep adaptation networks. In *International conference on machine learning*, pages 97–105. PMLR, 2015.
- Tim Marrinan, J Ross Beveridge, Bruce Draper, Michael Kirby, and Chris Peterson. Finding the subspace mean or median to fit your need. In *CVPR*, pages 1082–1089, 2014.
- John P Miller, Rohan Taori, Aditi Raghunathan, Shiori Sagawa, Pang Wei Koh, Vaishal Shankar, Percy Liang, Yair Carmon, and Ludwig Schmidt. Accuracy on the line: on the strong correlation between out-of-distribution and in-distribution generalization. In *International Conference on Machine Learning*, pages 7721–7735. PMLR, 2021.
- Krikamol Muandet, David Balduzzi, and Bernhard Schölkopf. Domain generalization via invariant feature representation. In *International Conference on Machine Learning*, pages 10–18, 2013.
- Giambattista Parascandolo, Alexander Neitz, Antonio Orvieto, Luigi Gresele, and Bernhard Schölkopf. Learning explanations that are hard to vary. *arXiv preprint arXiv:2009.00329*, 2020.
- Karl Pearson. On lines and planes of closest fit to systems of points in space. *The London, Edinburgh, and Dublin philosophical magazine and journal of science*, 2(11):559–572, 1901.
- F. Pedregosa, G. Varoquaux, A. Gramfort, V. Michel, B. Thirion, O. Grisel, M. Blondel, P. Prettenhofer, R. Weiss, V. Dubourg, J. Vanderplas, A. Passos, D. Cournapeau, M. Brucher, M. Perrot, and E. Duchesnay. Scikit-learn: Machine learning in Python. *Journal of Machine Learning Research*, 12:2825–2830, 2011.
- Jonas Peters, Peter Bühlmann, and Nicolai Meinshausen. Causal inference using invariant prediction: identification and confidence intervals, 2015.

- Alec Radford, Jong Wook Kim, Chris Hallacy, Aditya Ramesh, Gabriel Goh, Sandhini Agarwal, Girish Sastry, Amanda Askell, Pamela Mishkin, Jack Clark, et al. Learning transferable visual models from natural language supervision. In *International Conference on Machine Learning*, pages 8748–8763. PMLR, 2021.
- Elan Rosenfeld, Pradeep Kumar Ravikumar, and Andrej Risteski. The risks of invariant risk minimization. In *International Conference on Learning Representations*, 2021. URL <https://openreview.net/forum?id=BbNIbVPJ-42>.
- Elan Rosenfeld, Pradeep Ravikumar, and Andrej Risteski. Domain-adjusted regression or: Erm may already learn features sufficient for out-of-distribution generalization. *arXiv preprint arXiv:2202.06856*, 2022.
- Shiori Sagawa, Pang Wei Koh, Tatsunori B Hashimoto, and Percy Liang. Distributionally robust neural networks for group shifts: On the importance of regularization for worst-case generalization. *arXiv preprint arXiv:1911.08731*, 2019.
- Zheyang Shen, Jiashuo Liu, Yue He, Xingxuan Zhang, Renzhe Xu, Han Yu, and Peng Cui. Towards out-of-distribution generalization: A survey. *arXiv preprint arXiv:2108.13624*, 2021.
- Claudia Shi, Victor Veitch, and David Blei. Invariant representation learning for treatment effect estimation. *arXiv preprint arXiv:2011.12379*, 2020.
- Sahil Singla and Soheil Feizi. Salient imagenet: How to discover spurious features in deep learning? In *International Conference on Learning Representations*, 2021.
- Baochen Sun and Kate Saenko. Deep coral: Correlation alignment for deep domain adaptation. In *European conference on computer vision*, pages 443–450. Springer, 2016.
- Remi Tachet des Combes, Han Zhao, Yu-Xiang Wang, and Geoffrey J Gordon. Domain adaptation with conditional distribution matching and generalized label shift. *Advances in Neural Information Processing Systems*, 33:19276–19289, 2020.
- Eric Tzeng, Judy Hoffman, Kate Saenko, and Trevor Darrell. Adversarial discriminative domain adaptation. In *CVPR*, pages 7167–7176, 2017.
- Vladimir Vapnik. Principles of risk minimization for learning theory. In *Advances in neural information processing systems*, pages 831–838, 1992.
- Riccardo Volpi, Hongseok Namkoong, Ozan Sener, John C. Duchi, Vittorio Murino, and Silvio Savarese. Generalizing to unseen domains via adversarial data augmentation. In *NeurIPS*, pages 5339–5349, 2018.
- Vincent Q Vu, Juhee Cho, Jing Lei, and Karl Rohe. Fantope projection and selection: A near-optimal convex relaxation of sparse pca. *Advances in neural information processing systems*, 26, 2013.
- Catherine Wah, Steve Branson, Peter Welinder, Pietro Perona, and Serge Belongie. The caltech-ucsd birds-200-2011 dataset. 2011.

- Haixiang Wang, Han Zhao, and Bo Li. Bridging multi-task learning and meta-learning: Towards efficient training and effective adaptation. In *International Conference on Machine Learning*, pages 10991–11002. PMLR, 2021a.
- Haixiang Wang, Bo Li, and Han Zhao. Understanding gradual domain adaptation: Improved analysis, optimal path and beyond. In *International Conference on Machine Learning*, pages 22784–22801. PMLR, 2022a.
- Haixiang Wang, Yite Wang, Ruoyu Sun, and Bo Li. Global convergence of maml and theory-inspired neural architecture search for few-shot learning. *CVPR*, 2022b.
- Jindong Wang, Cuiling Lan, Chang Liu, Yidong Ouyang, Wenjun Zeng, and Tao Qin. Generalizing to unseen domains: A survey on domain generalization. *arXiv preprint arXiv:2103.03097*, 2021b.
- Olivia Wiles, Sven Gowal, Florian Stimberg, Sylvestre Alvisé-Rebuffi, Ira Ktena, Taylan Cemgil, et al. A fine-grained analysis on distribution shift. *arXiv preprint arXiv:2110.11328*, 2021.
- Adina Williams, Nikita Nangia, and Samuel R Bowman. A broad-coverage challenge corpus for sentence understanding through inference. *arXiv preprint arXiv:1704.05426*, 2017.
- Mitchell Wortsman, Gabriel Ilharco, Jong Wook Kim, Mike Li, Simon Kornblith, Rebecca Roelofs, Raphael Gontijo Lopes, Hannaneh Hajishirzi, Ali Farhadi, Hongseok Namkoong, and Ludwig Schmidt. Robust fine-tuning of zero-shot models. In *Proceedings of the IEEE/CVF Conference on Computer Vision and Pattern Recognition*, pages 7959–7971, 2022.
- Huaxiu Yao, Yiping Wang, Linjun Zhang, James Zou, and Chelsea Finn. C-mixup: Improving generalization in regression. In *Proceeding of the Thirty-Sixth Conference on Neural Information Processing Systems*, 2022a.
- Huaxiu Yao, Yiping Wang, Linjun Zhang, James Y Zou, and Chelsea Finn. C-mixup: Improving generalization in regression. *Advances in Neural Information Processing Systems*, 35:3361–3376, 2022b.
- Haotian Ye, Chuanlong Xie, Tianle Cai, Ruichen Li, Zhenguo Li, and Liwei Wang. Towards a theoretical framework of out-of-distribution generalization. In A. Beygelzimer, Y. Dauphin, P. Liang, and J. Wortman Vaughan, editors, *Advances in Neural Information Processing Systems*, 2021.
- Mao Ye, Ruichen Jiang, Haixiang Wang, Dhruv Choudhary, Xiaocong Du, Bhargav Bhushanam, Aryan Mokhtari, Arun Kejariwal, and qiang liu. Future gradient descent for adapting the temporal shifting data distribution in online recommendation system. In *The 38th Conference on Uncertainty in Artificial Intelligence*, 2022.
- Guojun Zhang, Han Zhao, Yaoliang Yu, and Pascal Poupart. Quantifying and improving transferability in domain generalization. In A. Beygelzimer, Y. Dauphin, P. Liang, and J. Wortman Vaughan, editors, *Advances in Neural Information Processing Systems*, 2021.

- Michael Zhang, Nimit S Sohoni, Hongyang R Zhang, Chelsea Finn, and Christopher Ré. Correct-n-contrast: A contrastive approach for improving robustness to spurious correlations. *arXiv preprint arXiv:2203.01517*, 2022.
- Han Zhao, Shanghang Zhang, Guanhang Wu, José MF Moura, Joao P Costeira, and Geoffrey J Gordon. Adversarial multiple source domain adaptation. *Advances in neural information processing systems*, 31:8559–8570, 2018.
- Han Zhao, Remi Tachet Des Combes, Kun Zhang, and Geoffrey Gordon. On learning invariant representations for domain adaptation. In *International Conference on Machine Learning*, pages 7523–7532. PMLR, 2019.
- Bolei Zhou, Agata Lapedriza, Aditya Khosla, Aude Oliva, and Antonio Torralba. Places: A 10 million image database for scene recognition. *IEEE transactions on pattern analysis and machine intelligence*, 40(6):1452–1464, 2017.
- Kaiyang Zhou, Ziwei Liu, Yu Qiao, Tao Xiang, and Chen Change Loy. Domain generalization: A survey. *arXiv preprint arXiv:2103.02503*, 2021.

A. Proof

A.1 Proof of Theorem 1

Proof From (17), we know

$$\mathcal{M} := \begin{bmatrix} \bar{x}_1^\top \\ \vdots \\ \bar{x}_E^\top \end{bmatrix} = \begin{bmatrix} \mu_c^\top A^\top + \mu_1^\top B^\top \\ \vdots \\ \mu_c^\top A^\top + \mu_E^\top B^\top \end{bmatrix} = \overbrace{\begin{bmatrix} \mu_c^\top & \mu_1^\top \\ \vdots & \vdots \\ \mu_c^\top & \mu_E^\top \end{bmatrix}}^{\mathcal{U}^\top} R^\top = (R\mathcal{U})^\top \quad (33)$$

where $\mathcal{U} := \begin{bmatrix} \mu_c & \cdots & \mu_c \\ \mu_1 & \cdots & \mu_E \end{bmatrix} \in \mathbb{R}^{d \times E}$

If $E \leq d_s$, Assumption 1 guarantees that $\{\mu_1, \dots, \mu_E\}$ are linearly independent almost surely. Then, we have $\text{rank}(\mathcal{U}) = E$. As $E > d_s$, since the first d_c rows of \mathcal{U} are the same, the rank of \mathcal{U} is capped, i.e., $\text{rank}(\mathcal{U}) = d - d_c = d_s$.

The mean-subtraction step of PCA compute the sample-mean

$$\tilde{x} = \frac{1}{E} \sum_{e=1}^E \bar{x}_e = A\mu_c + B \left(\frac{1}{E} \sum_{e=1}^E \mu_e \right) = A\mu_c + B\bar{\mu}, \quad (34)$$

where $\bar{\mu} := \frac{1}{E} \sum_{e=1}^E \mu_e$, and then subtracts \tilde{x}^\top off each row of \mathcal{M} to obtain

$$\tilde{\mathcal{M}} := \begin{bmatrix} \bar{x}_1^\top - \tilde{x}^\top \\ \vdots \\ \bar{x}_E^\top - \tilde{x}^\top \end{bmatrix} = \begin{bmatrix} (\mu_1 - \bar{\mu})^\top B^\top \\ \vdots \\ (\mu_E - \bar{\mu})^\top B^\top \end{bmatrix} = \overbrace{\begin{bmatrix} \mu_1^\top - \bar{\mu}^\top \\ \vdots \\ \mu_E^\top - \bar{\mu}^\top \end{bmatrix}}^{\tilde{\mathcal{U}}^\top} B^\top = (B\tilde{\mathcal{U}})^\top \in \mathbb{R}^{d_s \times d} \quad (35)$$

where $\tilde{\mathcal{U}} := [\mu_1 - \bar{\mu} \quad \dots \quad \mu_E - \bar{\mu}] \in \mathbb{R}^{d_s \times E}$

Similar to the analysis of \mathcal{U} above, we can also analyze the rank of $\tilde{\mathcal{U}}$ in the same way. However, different from \mathcal{U} , we have $\text{rank}(\tilde{\mathcal{U}}) = \min\{d_s, E - 1\}$, where the -1 comes from the constraint $\sum_{e=1}^E (\mu_e - \bar{\mu}) = 0$ that is put by the mean-subtraction.

Suppose $E \geq d_s + 1$, then $\text{rank}(\tilde{\mathcal{U}}) = d_s$. The next step of PCA is to eigen-decompose the sample covariance matrix

$$\begin{aligned} \frac{1}{E} \tilde{\mathcal{M}}^\top \tilde{\mathcal{M}} &= \frac{1}{E} (B\tilde{\mathcal{U}})(B\tilde{\mathcal{U}})^\top = \frac{1}{E} B(\tilde{\mathcal{U}}\tilde{\mathcal{U}}^\top)B^\top \\ &= \frac{1}{E} \begin{bmatrix} A & B \end{bmatrix} \begin{bmatrix} \mathbf{0}_{d_c \times d_c} & \mathbf{0}_{d_c \times d_s} \\ \mathbf{0}_{d_s \times d_c} & \tilde{\mathcal{U}}\tilde{\mathcal{U}}^\top \end{bmatrix} \begin{bmatrix} A^\top \\ B^\top \end{bmatrix} \in \mathbb{R}^{d \times d} \end{aligned} \quad (36)$$

where $\mathbf{0}_{n \times m}$ is a $n \times m$ matrix with all zero entries, and $\tilde{\mathcal{U}}\tilde{\mathcal{U}}^\top \in \mathbb{R}^{d_s \times d_s}$ is full-rank because $\text{rank}(\tilde{\mathcal{U}}) = d_s$.

Combining with the fact that $R = [AB]$ is full-rank (ensured by Assumption 3), we know that $\text{rank}(\frac{1}{E} \tilde{\mathcal{M}}^\top \tilde{\mathcal{M}}) = d_s$. Therefore, $\frac{1}{E} \tilde{\mathcal{M}}^\top \tilde{\mathcal{M}}$ is positive-definite.

As a result, the eigen-decomposition on $\frac{1}{E} \tilde{\mathcal{M}}^\top \tilde{\mathcal{M}}$ leads to an eigen-spectrum of d_s positive values and $d_c = d - d_s$ zero eigenvalues.

Consider ascendingly ordered eigenvalues $\{\lambda_1, \dots, \lambda_d\}$, and compose a diagonal matrix S with these eigenvalues as in ascending order, i.e., $S := \text{diag}(\{\lambda_1, \dots, \lambda_d\})$. Denote the eigenvectors corresponding with these eigenvalues as $\{P_1, \dots, P_{d_c}\}$, and stack their transposed matrices as

$$P := \begin{bmatrix} P_1^\top \\ \vdots \\ P_{d_c}^\top \end{bmatrix} \in \mathbb{R}^{d \times d} \quad (37)$$

Then, we have the equality

$$\frac{1}{E} B(\tilde{U}\tilde{U}^\top)B^\top = \frac{1}{E} \tilde{M}^\top \tilde{M} = PSP^\top \quad (38)$$

Since the first d_c diagonal entries of S are all zeros and the rest are all non-zero, the dimensions of P that correspond to non-zero diagonal entries of S can provide us with the subspace spanned by the d_s spurious latent feature dimensions, thus the rest dimensions of P (i.e., the ones with zero eigenvalues) correspond to the subspace spanned by d_c invariant latent feature dimensions, i.e.,

$$\text{Span}(\{P_i^\top R : i \in [d], S_{ii} = 0\}) = \text{Span}(\{\hat{\mathbf{d}}_c^1, \dots, \hat{\mathbf{d}}_c^{d_c}\}) \quad (39)$$

Since the diagonal entries of S are sorted in ascending order, we can equivalently write it as

$$\text{Span}(\{P_1^\top R, \dots, P_{d_c}^\top R\}) = \text{Span}(\{\hat{\mathbf{d}}_c^1, \dots, \hat{\mathbf{d}}_c^{d_c}\}) \quad (40)$$

Then, by Proposition 1 (i.e., Definition 1 of Rosenfeld et al. (2021)) and Lemma F.2 of Rosenfeld et al. (2021), for the ERM predictor fitted to all data that are projected to the recovered subspace, we know it is guaranteed to be the optimal invariant predictor (defined in Proposition 1 as Eq. (12)).

Case $E \leq d_s$ Now, let us consider the case when $E \leq d_s$, $\text{rank}(\hat{U}) = \min(E - 1, d_s) = E - 1$. The eigen-decomposition of $\tilde{M}^\top \tilde{M}$ will yield $E - 1$ strictly positive eigenvalues and $d - (E - 1) > d_c$ zero eigenvalues. In this case,

$$\text{Span}(\{P_i^\top R : P_i \in P_{zero}\}) \supset \text{Span}(\{\hat{\mathbf{d}}_c^1, \dots, \hat{\mathbf{d}}_c^{d_c}\}) \quad (41)$$

where P_{zero} belongs to the set of eigenvectors corresponding to zero eigenvalues. One could alternately leverage the transformation matrix obtained by stacking eigenvectors in $P_{positive}$ (set of eigenvectors corresponding to strictly positive eigenvalues) i.e. $[P_1, \dots, P_{E-1}]^\top = P'' \in \mathbb{R}^{(E-1) \times d}$ to *partially* recover the spurious feature subspace:

$$\text{Span}(\{P_i^\top R : P_i \in P_{positive}\}) \subset \text{Span}(\{\hat{\mathbf{d}}_s^1, \dots, \hat{\mathbf{d}}_s^{d_s}\}) \quad (42)$$

Following this, the nullspace of P'' can be used to obtain $\text{Nullspace}(P'') = P' \in \mathbb{R}^{(d-(E-1)) \times d}$ to recover a *partial* transformation to the invariant-feature subspace under the available information. While both of these present two ways to recover the invariant-feature subspace, it is suggested to use equation (42), which only removes those spurious dimensions that *significantly vary* across environments. ■

A.2 Proof of Theorem 2

Proof From (20), we know

$$\Delta\Sigma := \Sigma_{e_1} - \Sigma_{e_2} = (\sigma_{e_1}^2 - \sigma_{e_2}^2)BB^\top \in \mathbb{R}^{d \times d} \quad (43)$$

Assumption 2 guarantees that $\sigma_{e_1}^2 - \sigma_{e_2}^2 \neq 0$, and Assumption 3 ensures that $\text{rank}(B) = d_s$. Thus, eigen-decomposition on $\Delta\Sigma$ leads to exactly d_c zero eigenvalues and $d_s = 1 - d_c$ non-zero eigenvalues. One just need to follow the same steps as (36)-(40) to finish the proof. ■

A.3 Proof of Theorem 3

Proof Consider the matrix \mathcal{M}_{total} as per (25):

$$\mathcal{M}_{total} := [P_1|P_2|\dots|P_k] \in \mathbb{R}^{d \times (E-1)k} \quad (44)$$

By definition, $\text{rank}(\mathcal{M}_{total}) \leq \min(d, (E-1) \times k)$, which trivially implies:

$$\text{rank}(\mathcal{M}_{total}) \leq (E-1) \times k \quad (45)$$

Recall that each P_k recovers the spurious dimension specific to class k . In order to recover the underlying d_s dimensional subspace, the rank of $\mathcal{M}_{total} = d_s$. Combining this fact with the above statement, the following inequality is obtained:

$$E - 1 \geq d_s/k \quad (46)$$

$$E \geq d_s/k + 1 \quad (47)$$

Thus, the minimum number of environments required to recover the spurious (thus invariant) feature subspace *benefits* by leveraging information from classes. The greater the number of classes, the lesser the number of training environments we require to recover the d_c dimensional invariant features. It should be noted that this decrease is observed while only leveraging the 1st order moments of the class conditional data distribution.

Assuming condition 4 is satisfied, the rank of \mathcal{M}_{total} is capped at d_s . Thus, the SVD will lead to d_s strictly positive singular values. Then, one can obtain the d_s eigenvectors corresponding to these singular values, which span the spurious dimensions. The transformation matrix will be $P' \in \mathbb{R}^{d_s \times d}$. Since $z_s \perp z_c$ as per the setup 3.2, the null space of P' will correspond to vectors spanning the $d - d_s = d_c$ dimensions as follows:

$$\text{NullSpace}(P') = P'' \in \mathbb{R}^{d_c \times d} \quad (48)$$

Finally, training on this invariant subspace helps obtain the optimal invariant predictor as per 1, which completes the proof. ■

A.4 Proof of Theorem 4

Proof Consider the matrix \mathcal{M} as per (30):

$$\mathcal{M} := \begin{bmatrix} \bar{x}_1^\top \\ \vdots \\ \bar{x}_E^\top \end{bmatrix} \in \mathbb{R}^{E \times d} \quad (49)$$

Recall that under the infinite sample setting, each row \bar{x}_e^\top of \mathcal{M} can be represented as the following mean estimate:

$$\bar{x}_e = A\mu_c + B\mu_e \quad (50)$$

Thus, \mathcal{M} can now be expressed as:

$$\mathcal{M} := \begin{bmatrix} \bar{x}_1^\top \\ \vdots \\ \bar{x}_E^\top \end{bmatrix} = \begin{bmatrix} \mu_c^\top A^\top + \mu_1^\top B^\top \\ \vdots \\ \mu_c^\top A^\top + \mu_E^\top B^\top \end{bmatrix} = \overbrace{\begin{bmatrix} \mu_c^\top & \mu_1^\top \\ \vdots & \vdots \\ \mu_c^\top & \mu_E^\top \end{bmatrix}}^{U^\top :=} R^\top \quad (51)$$

where

$$U = \begin{bmatrix} \mu_c & \mu_c & \cdots & \mu_c \\ \mu_1 & \mu_2 & \cdots & \mu_E \end{bmatrix} \in \mathbb{R}^{d \times E} \quad (52)$$

Note that once we have this formulation, one can follow the same steps as the proof in Appendix A.1. which completes the proof. ■

B. Experimental Details

B.1 Setups of Synthetic Datasets

Example-2 This is a binary classification task that imitate the following example inspired by Arjovsky et al. (2019); Beery et al. (2018): while most cows appear in grasslands and most camels appear in deserts, with small probability such relationship can be flipped. In this example, Aubin et al. (2021) define the animals as invariant features with mean $\pm\mu_c$ and the backgrounds as spurious features with mean $\pm\mu_e$. Aubin et al. (2021) also scale the invariant and spurious features with ν_c and ν_e respectively. To be specific, we set $\mu_c = \mathbf{1}_{d_c}$ (i.e., a d_c -dimensional vector with all elements equal to 1) , $\mu_e = \mathbf{1}_{d_e}$, $\nu_c = 0.02$ and $\nu_e = 1$. For any training environment $e \in \mathcal{E}$, Aubin et al. (2021) construct its dataset \mathcal{D}_e by generating each input-label pair (x, y) in the following process:

$$\begin{aligned} j_e &\sim \text{Categorical}(p^e s^e, (1-p^e)s^e, p^e(1-s^e), (1-p^e)(1-s^e)) \\ z_c &\sim \begin{cases} +1 \cdot (\mu_c + \mathcal{N}_{d_c}(0, 0.1)) \cdot \nu_c & \text{if } j_e \in \{1, 2\}, \\ -1 \cdot (\mu_c + \mathcal{N}_{d_c}(0, 0.1)) \cdot \nu_c & \text{if } j_e \in \{3, 4\}, \end{cases} \\ z_e &\sim \begin{cases} +1 \cdot (\mu_e + \mathcal{N}_{d_s}(0, 0.1)) \cdot \nu_e & \text{if } j_e \in \{1, 4\}, \\ -1 \cdot (\mu_e + \mathcal{N}_{d_s}(0, 0.1)) \cdot \nu_e & \text{if } j_e \in \{2, 3\}, \end{cases} \end{aligned}$$

$$z \leftarrow \begin{bmatrix} z_c \\ z_e \end{bmatrix}, \quad y \leftarrow \begin{cases} 1 & \text{if } \mathbf{1}_{d_c}^\top z_c > 0, \\ 0 & \text{else} \end{cases}, \quad x = Rz \quad \text{with} \quad R = I_d,$$

where the background probabilities are $p^{e=0} = 0.95$, $p^{e=1} = 0.97$, $p^{e=2} = 0.99$ and the animal probabilities are $s^{e=0} = 0.3$, $s^{e=1} = 0.5$, $s^{e=2} = 0.7$. If there are more than three environments, the extra environment variables are drawn according to $p^e \sim \text{Unif}(0.9, 1)$ and $s^e \sim \text{Unif}(0.3, 0.7)$.

Example-3 This is a linear version of the spiral binary classification problem proposed by Parascandolo et al. (2020). In this example, Aubin et al. (2021) assign the first d_c dimensions of the features with an invariant, small-margin linear decision boundary, and the rest d_e dimensions have a changing, large-margin linear decision boundary. To be specific, for all environments, the d_c invariant features are sampled from a distribution with a constant mean, while the means are sampled from a Gaussian distribution for the d_e spurious features. In practice set $\gamma = 0.1 \cdot \mathbf{1}_{d_c}$, $\mu_e \sim \mathcal{N}(\mathbf{0}_{d_c}, I_{d_c})$, and $\sigma_c = \sigma_e = 0.1$, for all environments. For any training environment $e \in \mathcal{E}$, Aubin et al. (2021) construct its dataset \mathcal{D}_e by generating each input-label pair (x, y) in the following process:

$$y \sim \text{Bernoulli}\left(\frac{1}{2}\right),$$

$$z_c \sim \begin{cases} \mathcal{N}(+\gamma, \sigma_c I_{d_c}) & \text{if } y = 0, \\ \mathcal{N}(-\gamma, \sigma_c I_{d_c}) & \text{if } y = 1; \end{cases}$$

$$z_e \sim \begin{cases} \mathcal{N}(+\mu_e, \sigma_e I_{d_s}) & \text{if } y = 0, \\ \mathcal{N}(-\mu_e, \sigma_e I_{d_s}) & \text{if } y = 1; \end{cases}$$

$$z \leftarrow \begin{bmatrix} z_c \\ z_e \end{bmatrix}, \quad x = Rz \quad \text{with} \quad R = I_d$$

Example-3' As explained in Section 5.1.1, in order to make Example-3 follow Assumption 2, we slightly modify the variance of the features in Example-3 so that $\sigma_c = 0.1$ and $\sigma_e \sim \text{Unif}(0.1, 0.3)$. All the rest settings are unchanged.

Example-2s/3s/3s' In order to increase the difficulty of the tasks, we defined the ‘‘scrambled’’ variations of the three problems described above. To build the scrambled variations, we no longer use the identity matrix I_d as the transformation matrix R ; instead, a random orthonormal matrix $R \in \mathbb{R}^{d \times d}$ is applied to the features for all environments $e \in \mathcal{E}$. The random transformation matrix is built from a Gaussian matrix (see the code <https://github.com/facebookresearch/InvarianceUnitTests> of Aubin et al. (2021) for details).

Multiclass Linear Unit Test In this dataset, the target y is sampled from a multinomial distribution of uniform probability $1/k$, where k is the number of classes. Then, the first d_c invariant features are sampled from a Gaussian distribution where the mean depends on the class label. Similarly, the next d_s spurious features are sampled from a Gaussian distribution where the mean now depends on the class label *as well as* the environment label. This can be formulated as follows:

For a given environment e ,

$$y \sim \text{Multinomial} \left(\frac{1}{k} \right), \quad (53)$$

$$z_c \sim \left\{ \mathcal{N}(\mu_k, \sigma_c I_{d_c}) * \nu_{inv} \quad \text{for } y = k, \right. \quad (54)$$

$$z_e \sim \left\{ \mathcal{N}(\mu_{ke}, \sigma_e I_{d_s}) * \nu_{spu} \quad \text{for } y = k, \text{ env} = e, \right. \quad (55)$$

$$z \leftarrow \begin{bmatrix} z_c \\ z_e \end{bmatrix}, \quad x = Rz \quad (56)$$

Regression Linear Unit Test The dataset is generated as follows. For a given environment e ,

$$z_c \sim \left\{ \mathcal{N}(\mu_c, \sigma_c I_{d_c}) * \nu_{inv}, \right. \quad (57)$$

$$y \sim w_c^\top z_c + b_c, \quad (58)$$

$$z_e \sim (W_{cs}^e z_c + b_e) * \nu_{spu} \quad (59)$$

$$z \leftarrow \begin{bmatrix} z_c \\ z_e \end{bmatrix}, \quad x = Rz \quad (60)$$

B.2 Experiments on Synthetic Datasets

Code We adopt the codebase of Linear Unit-Tests (Aubin et al., 2021), which provide implementations of Example-2/2s/3/3s and multiple algorithms (including IRMv1, IGA, ERM, Oracle). This codebase is released at <https://github.com/facebookresearch/InvarianceUnitTests>.

Hyper-parameters Similar to Aubin et al. (2021), we perform a hyper-parameter search of 20 trials. For each trial, we train the algorithms on the training split of all environments for 10K full-batch Adam (Kingma and Ba, 2015) iterations. We run the search for ISR-Mean and ISR-Cov algorithms on all examples, and run the search for ERM, IGA (Koyama and Yamaguchi, 2020), IRMv1 (Arjovsky et al., 2019) and Oracle on Example-3' and Example-3s'. We choose the hyper-parameters that minimize the mean error over the validation split of all environments. The experiment results for ERM, IGA, IRMv1 and Oracle on Example-2, Example-2s, Example-3 and Example-3s are from (Aubin et al., 2021), thus we do not perform any search on them.

For Multiclass Linear Unit Tests, in our experiments, $\sigma_c = 0.1, \sigma_e = 0.1, d_s = 5, d_c = 5$. We sample 10,000 points per environment. k varies from 2 to 7. For all methods, we perform a hyperparameter search over 5 data seeds and 5 model trials. In every trial, we train the algorithm on the train split and use the Adam Kingma and Ba (2014) optimizer for optimization. The model with the least mean validation error across all environments is chosen.

Multi-Class Colored MNIST In this dataset, for every digit, the corresponding color is highly correlated in the training set. This correlation breaks during testing.

We directly employ the Multiclass Colored MNIST dataset, models and hyperparameters provided by Ahuja et al. (2021a) at <https://github.com/ahujak/IB-IRM>. For ERM, IB-ERM, IRM and IB-IRM, we run a sweep over hyperparameters using the grid as suggested

above. The best model is chosen by using train domain validation (Gulrajani and Lopez-Paz (2020)). ISR-Multiclass is applied on the last-layer over the classification weights to enable the invariant-feature subspace transformation. Note that ISR-Multiclass uses color labels as the group information, and we ensure this same definition applies to IRM to ensure a fair comparison.

B.3 Experiments on Real Datasets

Training We directly use models, hyper-parameters and running scripts provided by authors of Sagawa et al. (2019) in https://github.com/kohpangwei/group_DRO. Specifically, they use ResNets (He et al., 2016) for Waterbirds and CelebA, and deploy BERT (Devlin et al., 2019) for MultiNLI. We train the neural nets following the official running scripts¹³. over 10 random seeds for Waterbirds/CelebA/MultiNLI. Each run leads to one trained neural network selected on the epoch with the highest worst-group validation accuracy.

ISR-Mean There are only $E = 2$ environments for Waterbirds, CelebA and MultiNLI and ISR-Mean can only identify a $\min\{E - 1, d_s\}$ -dimensional spurious subspace. Thus we assume $d_s = 1$ for the three datasets when applying ISR-Mean.

ISR-Cov For real datasets, we do not know the d_s of the learned features, thus we have to treat d_s as a hyperparameter for Algorithm 2.

Numerical Techniques The feature space of learned models is usually of a high dimension (e.g., 2048 for ResNet-50 in Waterbirds/CelebA), while the features of training data usually live in a subspace (approximately). Thus, we typically apply dimension reduction to features through a PCA. Then, to overcome some numerical instability challenges, we apply ISRs in an equivalent approach: we first identify the spurious-feature subspace, and then reduces scales of features along the spurious-feature subspace. The final step of fitting linear predictors in Algorithm 1/2 is done by logistic regression solver provided in scikit-learn Pedregosa et al. (2011). But in some cases, we find that directly adapting the original predictor of the trained model also yields good performance.

13. Provided in <https://worksheets.codalab.org/worksheets/Ox621811fe446b49bb818293bae2ef88c0>